NeuroImage 49 (2010) 3132–3148

Contents lists available at ScienceDirect

NeuroImage

journal homepage: www.elsevier.com/locate/ynimg

# Identifying the brain's most globally connected regions

Michael W. Cole [a,b,c,*], Sudhir Pathak [c], Walter Schneider [c,d]

[a] Department of Psychology, Washington University in St. Louis, MO 63130, USA
[b] Department of Neuroscience and Center for the Neural Basis of Cognition, University of Pittsburgh, PA 15260, USA
[c] Learning Research and Development Center, University of Pittsburgh, PA 15260, USA
[d] Department of Psychology, University of Pittsburgh, PA 15260, USA

ARTICLE INFO

*Article history:*
Received 12 August 2009
Revised 7 October 2009
Accepted 1 November 2009
Available online 10 November 2009

ABSTRACT

Recent advances in brain connectivity methods have made it possible to identify hubs—the brain's most globally connected regions. Such regions are essential for coordinating brain functions due to their connectivity with numerous regions with a variety of specializations. Current structural and functional connectivity methods generally agree that default mode network (DMN) regions have among the highest global brain connectivity (GBC). We developed two novel statistical approaches using resting state functional connectivity MRI—weighted and unweighted GBC (wGBC and uGBC)—to test the hypothesis that the highest global connectivity also occurs in the cognitive control network (CCN), a network anti-correlated with the DMN across a variety of tasks. High global connectivity was found in both CCN and DMN. The newly developed wGBC approach improves upon existing methods by quantifying inter-subject consistency, quantifying the highest GBC values by percentage, and avoiding arbitrary connection strength thresholding. The uGBC approach is based on graph theory and includes many of these improvements, but still requires an arbitrary connection threshold. We found high GBC in several subcortical regions (e.g., hippocampus, basal ganglia) only with wGBC despite the regions' extensive anatomical connectivity. These results demonstrate the complementary utility of wGBC and uGBC analyses for the characterization of the most highly connected, and thus most functionally important, regions of the brain. Additionally, the high connectivity of both the CCN and the DMN demonstrates that brain regions outside primary sensory-motor networks are highly involved in coordinating information throughout the brain.



## Introduction

The brain is thought to have evolved from simple reflex circuits, bestowing flexibility on behavior by integrating specialized brain regions into coordinated networks. Perhaps reflecting our especially flexible behavioral repertoire, the human brain is estimated to have hundreds of specialized brain regions (Van Essen, 2004). However, it is unknown how these specialized regions are integrated so behavior can be coordinated. Recent research has found that some regions have much higher global brain connectivity (GBC) than others, perhaps reflecting their role in integrating brain activity in order to coordinate cognition and behavior (Achard et al., 2006; Buckner et al., 2009; Hagmann et al., 2008; Heuvel et al., 2008; Salvador et al., 2005a; Sporns et al., 2007).

Existing GBC methods, using both anatomical (Hagmann et al., 2008) and functional (Buckner et al., 2009) connectivity, have identified regions in the default mode network (DMN) as having the highest GBC. This high connectivity may reflect connections necessary to implement the wide variety of cognitive functions the network is involved in. Consistent with this notion, we hypothesized that another large-scale network implementing a variety of cognitive function, the cognitive control network (CCN), also has among the highest GBC.

The CCN has been reported in many studies of cognitive control processes, and is likely involved in coordinating networks of brain regions during novel and non-routine tasks (Cole and Schneider, 2007; Dosenbach et al., 2006). The DMN has been reported in studies of resting state activity, suggesting it is active "by default" (Raichle et al., 2001). However, the DMN is engaged by mind wandering (Mason et al., 2007), prospective and retrospective self-reflection (D'Argembeau et al., 2008), and memory retrieval (Buckner et al., 2005), suggesting that the 'default mode' involves ongoing processing of information for relevance to the self. The CCN is thought to consist of dorsolateral prefrontal cortex (DLPFC), rostrolateral prefrontal cortex (RLPFC), dorsal–caudal anterior cingulate cortex (ACC), pre-supplementary motor area (pre-SMA), inferior frontal junction (IFJ), posterior parietal cortex (PPC), pre-motor cortex (PMC), and anterior insula cortex (AIC). The DMN is thought to consist of posterior cingulate cortex (PCC), rostral anterior cingulate cortex (rACC), anterior temporal lobe (aTL), superior frontal cortex (SFC), and inferior parietal cortex (IPC). Importantly, the CCN and DMN are anti-correlated during task performance and uncorrelated at rest (Fox et al., 2005; Murphy et al., 2008) (Fig. 1A), suggesting they are relatively independent networks. We predicted, given their

* Corresponding author. Department of Psychology, Washington University in St. Louis, MO 63130, USA. Fax: +1 314 935 8790.
*E-mail address:* mwcole@mwcole.net (M.W. Cole).

1053-8119/$ – see front matter © 2009 Elsevier Inc. All rights reserved.
doi:10.1016/j.neuroimage.2009.11.001

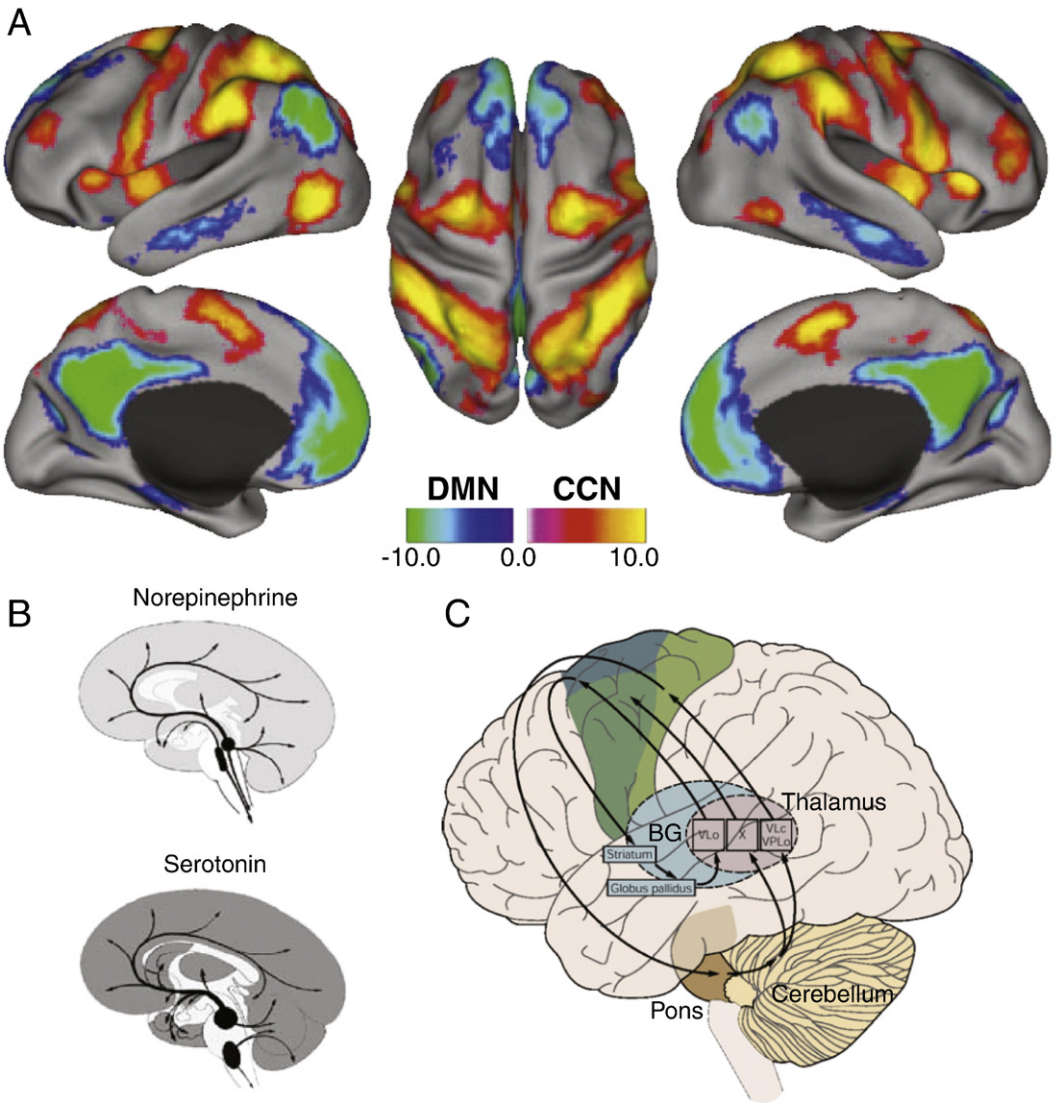


**Fig. 1.** Hypothesized globally connected circuits. (A) Previous research showed evidence for two large anti-correlated networks in cortex (Fox et al., 2005). Importantly, the functions of these networks suggest that they may have high global brain connectivity (GBC). The cognitive control network (CCN; yellow/red) and default mode network (DMN; blue/green) are thought to be involved in a wide variety of cognitive tasks. The depicted number scales are population *z*-scores (see Fox et al., 2005). Figure adapted from Fox et al. (2005). (B) Extensive work with animal models, and some with humans, has suggested that midbrain neurotransmitter systems project widely throughout the brain (Herlenius and Lagercrantz, 2004), and therefore are likely to have high GBC. Figure adapted from Herlenius and Lagercrantz (2004) and Squire et al. (2003). (C) Evidence from anatomical studies of basal ganglia (BG) shows that loops are formed throughout cortex (not just motor cortex (Middleton and Strick, 1994)), suggesting high GBC for the parts of BG looping with high GBC cortical regions. Anatomical loops have also been found between cerebellum and nearly all of cortex (Middleton and Strick, 1994), via the pons and thalamus, suggesting parts of cerebellum have high GBC as well. Figure adapted from Kandel et al. (2000).

involvement in a wide variety of complex cognitive behaviors that they would both have among the highest GBC in the human brain.

In addition to these two cortical networks, a variety of subcortical brain regions have been found in animal models to have high global connectivity. We predicted that these regions would also show high global connectivity in humans. One such region is amygdala, which is thought to integrate sensory and internal-state information for limbic processing (Barbas, 2000; Jolkkonen and Pitkänen, 1998). Similarly, hippocampal cortex (HC) is thought to integrate information from a wide variety of sources in order to encode entire episodes (Eichenbaum et al., 2007). Also, several midbrain neurotransmitter (MNT) regions such as locus coeruleus and substantia nigra are thought to project to a variety of regions throughout the brain (Fig. 1B) (Herlenius and Lagercrantz, 2004) and are thought to play important roles in motivation and arousal.

Another region, thalamus, includes several nuclei with differing connectivity profiles (Behrens et al., 2003), suggesting that only parts of it might have highly extensive connectivity. Similarly, basal ganglia (BG) and cerebellum connect with cortex via topographic loops (Kelly and Strick, 2003) (Fig. 1C), suggesting that some loops would bestow more wide-spread connectivity on parts of the structures than others. For these reasons, we predicted that amygdala and HC would have high global connectivity, as well as portions of thalamus, BG, and cerebellum.

Functional MRI (fMRI) is an increasingly important method for measuring functional connectivity non-invasively. Among the functional connectivity methods developed with fMRI, the decade-old method of resting state functional connectivity MRI (rs-fcMRI) is unique in its ability to capture functional connectivity largely independent of any particular brain state. Evidence for this comes from a study of anesthetized monkeys (Vincent et al., 2007) that showed rs-fcMRI patterns similar to humans at rest, as well as a study of rs-fcMRI during both task and rest in humans (Fair et al., 2007). Though further research is necessary, rs-fcMRI is thought to be based on very infrequent (~0.01 to 0.1 Hz) bursts of spiking activity in cortex that drive correlated activity through brain networks (Golanov et al., 1994; Kannurpatti et al., 2008).

In previous work, we observed that, since the entire brain is a network, the term *brain network* was ill defined. We developed a working definition of *brain network* as a set of regions with greater internal connectivity than external connectivity (Cole and Schneider, 2007). We were able to show using rs-fcMRI that the CCN fits this criterion. Importantly, we also found that the CCN is significantly more globally connected than the rest of the brain on average. Here we sought to replicate this finding with more refined methods, and also to determine what other brain regions exhibit high GBC. As outlined above, we predicted that the CCN, DMN, and a variety of subcortical regions would be among the most highly globally connected in the brain, perhaps reflecting their roles in coordinating complex cognitive behaviors.

Recently, another GBC method was developed that combines graph theory and rs-fcMRI with a whole-brain (voxel-wise) analysis approach (Buckner et al., 2009). Unlike the GBC method developed by Cole and Schneider (2007), the Buckner et al. (2009) method uses binary connections in an unweighted graph. In order to implement this unweighted GBC (uGBC) method a connection strength threshold is necessary which, unlike the weighted GBC (wGBC) method, involves removing connections with lower strength. Since wGBC does not require thresholding of the connection strengths, we predicted that it might reveal globally connected regions with many low-strength connections (such as modulatory subcortical regions; e.g., locus coeruleus) that might be removed by uGBC thresholding.

In order to compare the uGBC and wGBC methods, we implemented the whole-brain uGBC method (as developed by Buckner et al., 2009) and modified the wGBC method (as developed by Cole and Schneider, 2007) to also include whole-brain maps. We also modified both methods to be more statistically quantitative and accessible to a wider variety of researchers. Specifically, we applied widely used parametric statistical methodology to quantify inter-subject consistency, as well as a novel and easily interpretable thresholding approach that identifies the top percentages of voxels in terms of global connectivity. Thresholding the maps in terms of top percentage GBC allows comparison of the methods using a common metric despite differences between them.

A major motivation behind the development of these methods was to provide alternatives to graph theory for identifying the brain's most globally connected regions. Though graph theory has been quite productive in characterizing brain networks thus far (Bullmore and Sporns, 2009), as a branch of mathematics it typically does not

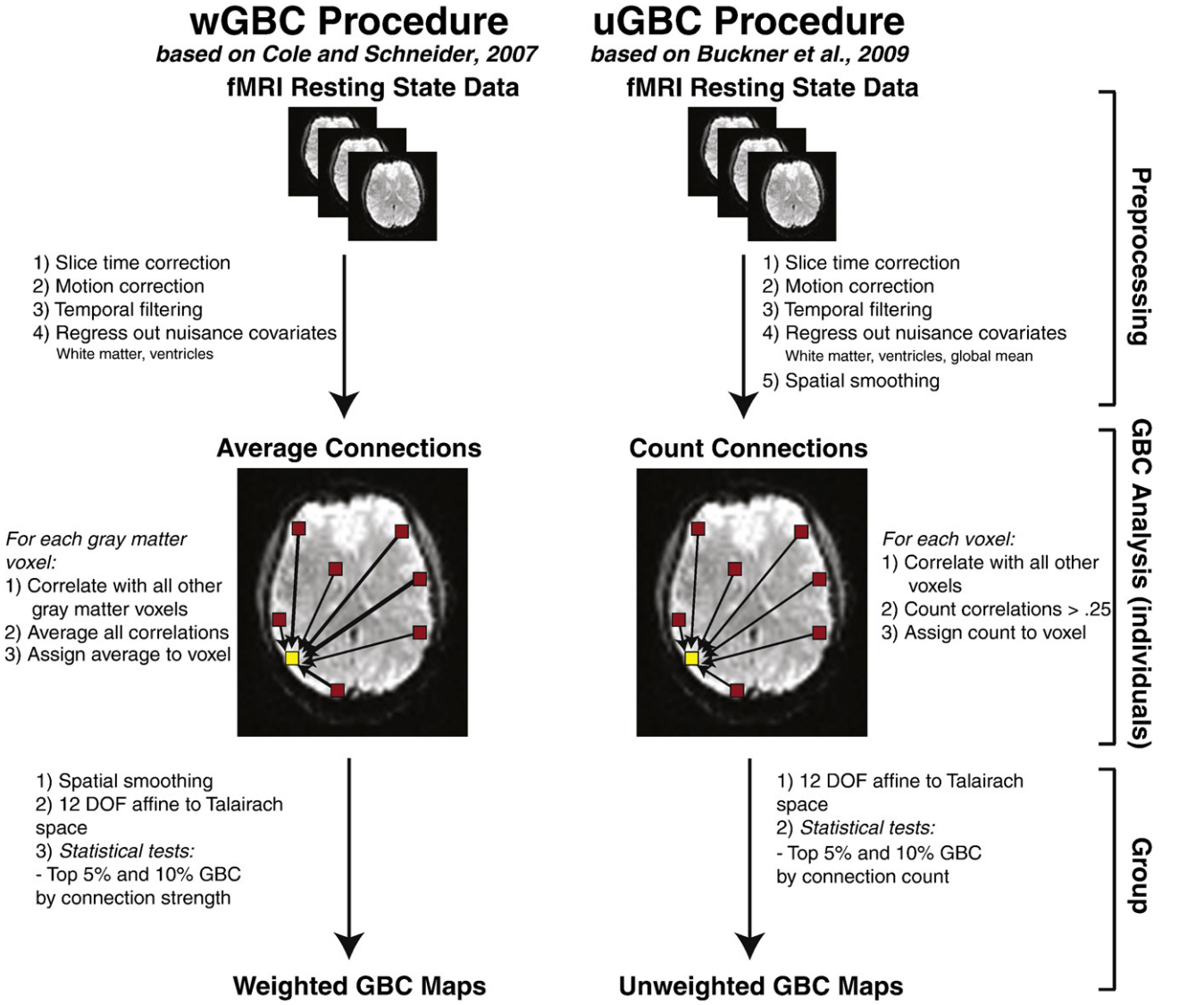


**Fig. 2.** GBC analysis methods. The GBC procedure based on Cole and Schneider (2007) is outlined on the left, while the procedure based on Buckner et al. (2009) is outlined on the right. GBC analysis involves assigning each gray matter voxel with its GBC, consisting either of the average correlation with all other gray matter voxels (wGBC) or the count of voxels above a certain threshold (uGBC).

quantify the statistical certainty of a given finding (Deuker et al., 2009; Kramer et al., 2009). Here we used statistical methods to quantify between-subject certainty, as well as the degree to which voxels are globally connected (in terms of percentages). We see these new approaches as complementary to graph theory, with the potential to increase confidence in brain network findings by acknowledging and quantifying the variability and graded nature of the data underlying those findings.

## Materials and methods

### *Participants*

We included 14 right-handed subjects (7 male, 7 female), aged 19 to 29 (mean age 22) in the study. These subjects were recruited from the University of Pittsburgh and surrounding area. Subjects were excluded if they had any medical, neurological, or psychiatric illness, any contraindications for MRI scans, or were left-handed. All subjects gave informed consent.

### *MRI data collection*

Image acquisition was carried out on a 3T Siemens Trio MRI scanner. Thirty-eight transaxial slices were acquired every 2000 ms (FOV: 205 mm, TE: 29 ms, Flip angle: 90°, voxel dimensions: $3.2 \times 3.2 \times 3.2$ mm), with a total of 300 echo-planar imaging (EPI) volumes collected per run. Siemens's implementation of generalized autocalibrating partially parallel acquisition (GRAPPA) was used to double the image acquisition speed (Griswold et al., 2002). Three-dimensional anatomical MP-RAGE images and T2 structural in-plane images were collected for each subject. One 10-min resting fMRI run was collected just after collecting anatomical images and before subjects performed any experimental tasks. A static white screen with a black central fixation cross was projected onto a screen visible to

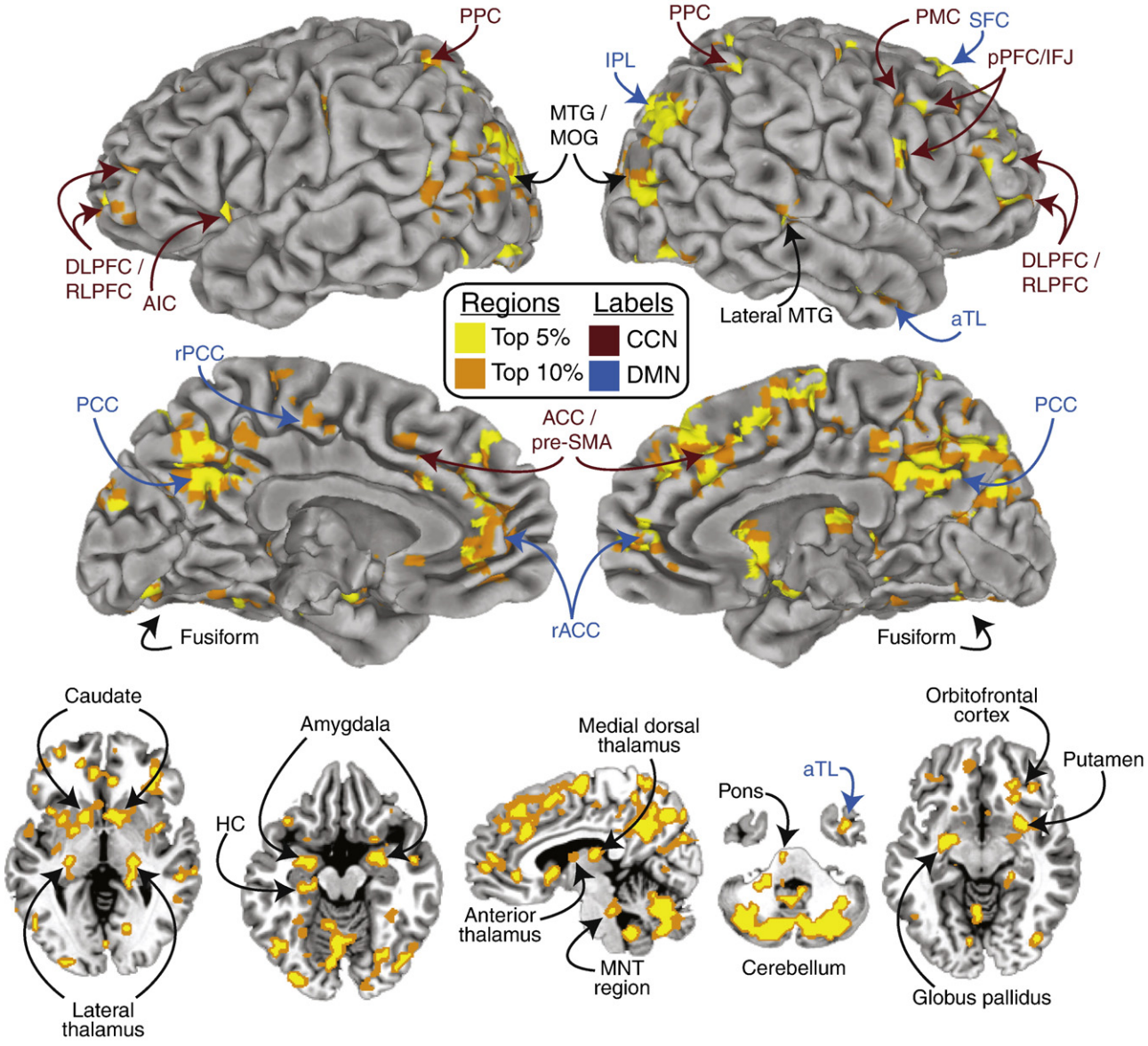


**Fig. 3.** Top percent wGBC regions. As hypothesized, the entire set of CCN (red) and DMN (blue) regions are among the most globally connected in the brain. Further, unlike uGBC, subcortical regions hypothesized to have high GBC show high wGBC. These regions include amygdala, hippocampal cortex (HC), the pons, a midbrain neurotransmitter (MNT) region (possibly locus coeruleus or the raphe nucleus), lateral thalamus, and the medial dorsal nucleus. Within the basal ganglia, the caudate and globus pallidus (extending into putamen) had high GBC. Finally, a large swath of cerebellum consistent with cerebellar–prefrontal circuits showed high GBC. The map was thresholded based on statistical confidence that each voxel is higher than an average correlation of 0 across subjects.

each subject via a mirror mounted inside the MRI scanner. Subjects were instructed to keep their eyes open (to avoid known eyes-closed oscillations in visual cortex (Goldman et al., 2002) and to help the subjects avoid falling asleep) with instructions to stay relaxed with eyes still.

### *Preprocessing*

Freesurfer (Dale et al., 1999; Fischl et al., 2002; Fischl et al., 2004) was used with each subject's MP-RAGE to segment gray matter, white matter, and ventricle voxels. Following this step, fMRI preprocessing, analysis, and visualization methods as implemented in AFNI and SUMA (Cox, 1996) were used. Activation maps were visualized either on a three-dimensional surface (using SUMA), or via slices with the activation interpolated to the template brain resolution (cubic spline interpolation; 1 $mm^3$). See Fig. 2 for an outline of the preprocessing steps.

Slice timing correction and motion correction procedures were used. Temporal filtering was applied with $0.009 < f(\text{Hz}) < 0.08$ in order to aid removal of nuisance cardiac and respiratory signals. Time series were then extracted from white matter and ventricle voxels (with some distance from the gray matter in order to ensure no overlap), and linear regression was used to remove any correlations between the gray matter voxels and these nuisance covariates (as well as their derivatives and the motion parameters). For the uGBC maps, the global signal was regressed out in order to replicate Buckner et al. (2009), who used global signal regression to remove potentially spurious physiological correlations. For the wGBC maps, the global signal was not regressed out in order to avoid potentially artifactual anti-correlations (Murphy et al., 2008), and also because this was a signal of interest. Note that both types of maps were qualitatively similar whether or not global signal regression was used. At present, there is some controversy regarding whether or not to perform global signal regression (Birn et al., 2006; Fox et al., 2009). We included a GBC method that uses global signal regression (uGBC) and one that does not (wGBC) in order to verify that any findings common to the two methods are independent of the methodological choices regarding global signal regression.

For the wGBC preprocessing, all voxels outside gray matter were masked out, while this step was not performed for uGBC since non-gray matter voxels (which have low correlations) are thresholded out as the uGBC maps are calculated. Further, including the non-gray matter values in the wGBC map would artificially lower the correlation averages, reducing the accuracy of the reported grand mean wGBC value. For similar reasons, spatial smoothing was not performed during wGBC preprocessing in order to avoid any contamination of the signals by non-gray matter sources prior to wGBC analysis. Smoothing (4 $mm^3$ FWHM) was applied for the uGBC preprocessing in order to replicate the method used by Buckner et al. (2009). Applying the spatial smoothing before and after uGBC processing produced qualitatively similar maps.

### *Weighted global brain connectivity (wGBC) analysis*

See the middle left portion of Fig. 2 for an outline of wGBC analysis. We developed the wGBC analysis method initially using MATLAB (The MathWorks, Natick, MA), switching to a more efficient function (AFNI's 3dTcorrMap) for the findings reported here. wGBC analysis involves seed-based correlation of each gray matter voxel with all other gray matter voxels. These values are then averaged together and the resulting value (i.e., that voxel's wGBC) is assigned to that voxel in a new brain map. Fisher's $z$ transformation is applied to each (Pearson's $r$) correlation prior to averaging, and then converted back to $r$-values afterward. This process repeats for all gray matter voxels, resulting in a single brain map per subject reflecting wGBC.

**Table 1**
Top 5% wGBC voxel clusters.

| Cluster labels | Hemisphere | Voxels (3.2 $mm^3$) | % Gray matter | *T*-statistic | Talairach coord: *x* | Talairach coord: *y* | Talairach coord: *z* | Brodmann areas |
|---|---|---|---|---|---|---|---|---|
| Cerebellum (posterior) | Both | 904 | 2.14 | 7.3819 | −4 | −62.2 | −28.2 | – |
| PCC | Both | 142 | 0.34 | 6.9067 | 1.2 | −55.3 | 32.4 | 31, 7, 23 |
| ACC/pre-SMA | Right | 118 | 0.28 | 7.1707 | 8.6 | 24.5 | 43.1 | 32, 24, 6, 8 |
| Putamen | Left | 73 | 0.17 | 7.0656 | −25.9 | −7.6 | 13.1 | – |
| MOG | Left | 46 | 0.11 | 6.9984 | −34.6 | −81.3 | 20.7 | 19, 18 |
| Amygdala | Left | 37 | 0.09 | 7.2606 | −22.4 | −6.3 | −7.1 | – |
| IPL | Right | 36 | 0.09 | 6.8059 | 41 | −70.2 | 32.8 | 39 |
| Caudate | Right | 32 | 0.08 | 6.822 | 10.9 | 9.1 | 3.1 | – |
| rACC | Left | 32 | 0.08 | 6.7971 | −6.4 | 40.3 | 19.4 | 32 |
| Amygdala | Right | 27 | 0.06 | 6.9174 | 25.8 | 1.1 | −10.3 | – |
| SFC | Left | 25 | 0.06 | 6.9676 | 26.3 | 26.2 | 35.2 | 8, 9 |
| aTL | Right | 21 | 0.05 | 6.7582 | 43.7 | 5.7 | −24.3 | 21, 22, 20 |
| Parahippocampus | Right | 21 | 0.05 | 7.0773 | 19.1 | −33.8 | 0.3 | 27 |
| RLPFC | Right | 21 | 0.05 | 6.8653 | 38.2 | 43.9 | 7.6 | 10 |
| SMA | Right | 21 | 0.05 | 7.136 | 6.8 | −9.6 | 59.6 | 6 |
| RLPFC | Left | 17 | 0.04 | 6.6956 | −32.3 | 49 | 5.9 | 10 |
| MTG | Left | 17 | 0.04 | 7.1264 | −44.2 | −62.3 | 4.3 | 37 |
| Orbitofrontal cortex | Right | 16 | 0.04 | 6.811 | 34.6 | 31.4 | −2.2 | 47, 11 |
| MOG | Right | 16 | 0.04 | 6.9992 | 41.6 | −76.8 | 8.4 | 19 |
| IFJ | Right | 16 | 0.04 | 6.6887 | 47.4 | 13.2 | 30 | 9, 6 |
| Orbitofrontal cortex | Right | 15 | 0.04 | 7.1105 | 21.9 | 27.7 | −4.7 | 11, 47 |
| rACC | Left | 15 | 0.04 | 7.1157 | 9.6 | 51.4 | 7.5 | 10, 32 |
| RLPFC | Right | 15 | 0.04 | 6.7635 | 35.5 | 42.7 | 21.3 | 10 |
| Cerebellum (tonsil) | Right | 14 | 0.03 | 7.0111 | 6.9 | −42.4 | −38.5 | – |
| Cerebellum (tonsil) | Left | 14 | 0.03 | 6.8211 | −3.6 | −52.8 | −37.8 | – |
| Inferior frontal gyrus | Right | 14 | 0.03 | 6.8487 | 53.7 | 6 | 19.2 | 44, 6 |
| Cerebellum (dentate) | Right | 12 | 0.03 | 7.0254 | 20.3 | −49.6 | −26.3 | – |
| AIC | Right | 12 | 0.03 | 6.9943 | 37.3 | 26.8 | 3.9 | 13, 45, 47 |
| IPL | Left | 12 | 0.03 | 6.9457 | −46.4 | −58.4 | 23.1 | 39 |
| PPC (precuneus) | Right | 11 | 0.03 | 6.6612 | 8.3 | −51.3 | 61.3 | 7 |
| Cerebellum (culmen) | Right | 10 | 0.02 | 6.7707 | 9.3 | −29.7 | −20.1 | – |
| Fusiform | Left | 10 | 0.02 | 6.7263 | −43.5 | −60.4 | −13 | 37 |

Cluster minimum for inclusion in table = 10 voxels. The percentage of gray matter included in the table equals 4.24%, due to the cluster minimum threshold (i.e., the remaining 0.76% are in clusters with fewer than 10 voxels).

In order to perform a group analysis, each subject's wGBC map was fit to a Talairach (Talairach, 1988) template (AFNI's version of 'colin27') using a 12 degrees-of-freedom affine transformation. Spatial smoothing (6 $mm^3$ FWHM) was then applied to the GBC map in order to help account for intersubject variability in the location and size of functional regions. Potential contamination across hemispheres due to spatial smoothing was avoided by applying smoothing to each hemisphere separately. The grand mean wGBC value for each subject was determined by averaging all the wGBC values across all gray matter voxels prior to Talairaching and spatial smoothing (reflecting the average wGBC across the brain).

*The wGBC statistical model*

A non-repeated measures ANOVA (with subjects as a random effect) was used to test hypotheses regarding the wGBC maps across the group. This group ANOVA compared each voxel's wGBC to zero, resulting in a statistical map quantifying the probability that there is a positive linear relationship between each voxel and all other voxels on average. The assumption made by the ANOVA of an approximately normal distribution between subjects was verified using normal Q–Q plots for the grand mean wGBC and the mean wGBC for an example region (PCC). ANOVA *p*-values for all statistical maps were calculated using the false discovery rate (FDR) correction for multiple comparisons (Genovese et al., 2002), and region identification was aided using the Talairach Daemon database (Lancaster et al., 2000) as implemented in AFNI.

The 'top percentage' threshold approach was developed in order to identify and quantify the voxels with the highest GBC. These thresholds were determined by raising the ANOVA threshold until the desired percentage (e.g., 5%) of the total gray matter voxels remained. The total number of gray matter voxels for the group (mean: 42,314, standard deviation: 1765), which was used to calculate all percentage thresholds, was determined by averaging across the total number of gray matter voxels of each subject. The number of gray matter voxels for each subject was estimated from their Freesurfer anatomical gray matter mask re-sampled as a functional volume (3.2 $mm^3$ voxels), Talairach-transformed, and dilated by one voxel. These binary masks were dilated by one voxel (i.e., binary 'smoothed' by 3.2 $mm^3$) as a conservative estimate of the effect of Gaussian spatial smoothing (which effectively increases the number of potentially correlating voxels) on the wGBC and uGBC results (smoothed by 6 $mm^3$ FWHM and 4 $mm^3$ FWHM, respectively). Since this was a conservative estimate, it is possible that the reported 'percentage of gray matter' values are actually slightly more selective than reported (e.g., the 'top 5%' may actually be the top 3%).

Note that the 'top percentage' threshold approach does not suffer from the multiple comparisons problem because it does not use statistical probability (i.e., *p*-values) for threshold selection. Rather, the proportion of gray matter voxels above each *F*-value threshold is used. Nonetheless, we corrected for multiple comparisons using FDR when reporting *p*-values associated with each threshold in order to remain statistically conservative. Only the reported *p*-values, not the statistical maps, were affected by the FDR corrections.

*Unweighted global brain connectivity (uGBC) analysis*

See the middle right portion of Fig. 2 for an outline of uGBC analysis. This method was a replication of the method developed by Buckner et al. (2009), which was based on previously developed graph theoretical approaches (e.g., Salvador et al., 2005b). uGBC

**Table 2**
Top 10% wGBC voxel clusters.

| Cluster labels | Hemisphere | Voxels (3.2 $mm^3$) | % Gray matter | Talairach coord: *x* | Talairach coord: *y* | Talairach coord: *z* | Brodmann areas |
|---|---|---|---|---|---|---|---|
| Cerebellum | Both | 1628 | 3.85 | −2.8 | −63.1 | −25.9 | – |
| PC/PCC | Both | 367 | 0.87 | 0.1 | −55.9 | 34.6 | 31, 7, 23 |
| RLPFC, VLPFC, AIC, caudate | Right | 288 | 0.68 | 30.2 | 29.2 | 6.8 | 10, 46, 45, 47, 13 |
| Putamen, globus pallidus, mid-insula | Left | 285 | 0.67 | −25 | −0.3 | 2.6 | 13 |
| ACC/pre-SMA | Right | 255 | 0.60 | 7.8 | 19.8 | 44.7 | 32, 24, 6, 8 |
| rACC | Both | 246 | 0.58 | −2.2 | 41.9 | 15.8 | 32, 24, 9, 10 |
| MTG/MOG | Left | 136 | 0.32 | −38.8 | −75.8 | 20.4 | 19, 39 |
| Amygdala, putamen, globus pallidus | Right | 112 | 0.26 | 28 | −3.2 | −4.5 | – |
| IPL | Right | 92 | 0.22 | 36.5 | −69.1 | 32.1 | 39 |
| pPFC/IFJ | Right | 86 | 0.20 | 47.1 | 11.4 | 25 | 9, 6 |
| Cuneus | Left | 68 | 0.16 | −1.2 | −83.5 | 23.3 | 18 |
| aTL | Right | 64 | 0.15 | 43 | 4 | −25.9 | 21, 22, 20 |
| RLPFC | Left | 64 | 0.15 | −33.6 | 47 | 7.8 | 10 |
| SFC | Right | 50 | 0.12 | 26 | 29.4 | 34.8 | 8, 9 |
| Lateral geniculate thalamus, pulvinar, parahippocampus | Right | 46 | 0.11 | 18.6 | −31.2 | 0.6 | 35, 30, 27 |
| MTG/MOG | Right | 46 | 0.11 | 37.5 | −79.4 | 12 | 19, 18, 39 |
| Precuneus | Right | 41 | 0.10 | 9.9 | −55.4 | 58.7 | 7 |
| PCC | Right | 35 | 0.08 | 11 | −65.5 | 13.6 | 31, 30 |
| S1/M1 | Left | 31 | 0.07 | −48.5 | −18.6 | 34.5 | 3, 4, 2 |
| PPC | Right | 31 | 0.07 | 40.9 | −42.3 | 44.8 | 40, 7 |
| Medial dorsal thalamus | Right | 28 | 0.07 | 7.3 | −19.7 | 12.8 | – |
| Superior temporal gyrus/posterior insula | Right | 27 | 0.06 | 49.1 | −32.3 | 16.4 | 41, 13 |
| Lateral MTG | Right | 26 | 0.06 | 57 | −29.6 | 1.1 | 21, 22 |
| SFG | Left | 23 | 0.05 | −31.4 | 32.8 | 30.1 | 8, 9 |
| Lateral MTG | Left | 22 | 0.05 | −53.9 | −50.9 | 10.4 | 22 |
| Superior temporal gyrus/posterior insula | Left | 20 | 0.05 | −36 | −29 | 12.8 | 41, 13 |
| Fusiform | Right | 19 | 0.04 | 32.2 | −41.9 | −16.5 | 20 |
| HC (hippocampus, parahippocampus) | Left | 19 | 0.04 | −22.8 | −22.9 | −13 | 35 |
| Lateral geniculate thalamus, parahippocampus | Left | 19 | 0.04 | −22 | −28 | 0 | 30, 27 |
| IPL | Left | 19 | 0.04 | −34.5 | −68.7 | 42.1 | 7, 19 |
| rPCC | Both | 19 | 0.04 | −2.3 | −17.4 | 48 | 31, 6 |
| PMC | Left | 17 | 0.04 | −41.6 | 3.2 | 41.3 | 6 |

Minimum cluster size = 15 voxels. The percentage of gray matter included in the table equals 9.99%, due to the cluster minimum threshold (i.e., the remaining 0.01% are in clusters with fewer than 15 voxels).

analysis involves calculating a seed correlation map of each voxel to all other voxels, with each voxel's degree of connectivity (i.e., number of connections) assigned to that voxel in the resulting map. Each seed correlation map is thresholded at a given value (here, as in Buckner et al., 2009, $r>0.25$) in order to remove low correlations that may be present due to noise. One uGBC map was created per subject, and that map was $z$-normalized in order to account for differences in brain size. $Z$-normalization involved subtracting the across-voxel mean from each voxel and dividing by the across-voxel standard deviation. The uGBC maps were then fit to a Talairach (Talairach and Tournoux, 1988) template (AFNI's version of 'colin27') using a 12 degrees-of-freedom affine transformation.

*The uGBC statistical model*

Unlike Buckner et al. (2009), statistical inference was used to ensure reliability across subjects. Specifically, a non-repeated measures ANOVA (with subjects as a random effect) was used to test hypotheses regarding the uGBC maps across the group. This group ANOVA compared each voxel's uGBC to zero (i.e., the mean number of connections), resulting in a statistical map quantifying the probability that each voxel has more connections than the average voxel. The assumption made by the ANOVA of an approximately normal distribution between subjects was verified using normal quantile–quantile (Q–Q) plots for the grand mean uGBC and the mean uGBC for an example region (PCC). All additional steps were identical to those of the wGBC method.

*GBC distribution analyses*

The group distributions were visualized using histograms and normal Q–Q plots (using R (R Development Core Team, 2008)) of the GBC values from all gray matter voxels for all subjects. Individual subject wGBC and uGBC data were $z$-normalized prior to combining with the group data. Data were also plotted from two example subjects in order to illustrate the similarity between the group distributions and those of the individual subjects.

## Results

*Grand mean global connectivity strength*

The group mean global connectivity strength across all gray matter voxels (i.e., the group grand mean wGBC) was $r=0.035$, with a standard deviation (between subjects) of 0.0198. All subjects had low, yet positive grand mean wGBC, suggesting brain regions are positively correlated on average.

*Top percent wGBC*

As expected, all CCN and DMN regions were included in the top 5% ($p<0.00016$, FDR corrected) of wGBC voxels. Additionally, several subcortical regions expected to have among the highest GBC are present. These subcortical regions include amygdala, HC, medial dorsal thalamus, an MNT region, cerebellum, globus pallidus, caudate, and lateral thalamus. These results are detailed in Fig. 3, and Tables 1 and 2.

*Top percent uGBC*

As expected, the majority of the top uGBC regions were either in the CCN or DMN. The top 5% of voxels were statistically significant with <0.0154 (FDR corrected). These results are detailed in Fig. 4, and Tables 3 and 4. All CCN regions were included, while nearly all DMN regions (with the exception of aTL) were included. Additional regions included middle temporal gyrus (MTG), middle occipital gyrus (MOG), and ventro-lateral prefrontal cortex (VLPFC; which may be part of the CCN). Note the absence of any subcortical regions at 5%. The top 10% of uGBC voxels (Fig. 4; $p<0.0328$, FDR corrected) are highly consistent with the results at 5%. Importantly, the DMN region missing at 5% (aTL) is present at 10%, as well as two small regions in cerebellum.

*Conjunction of wGBC and uGBC results*

A conjunction map was created between the wGBC and uGBC results at the top 5% and 10% (Fig. 5 and Table 5). For the 'top 5%', all voxels common to wGBC and uGBC in their respective top 5% maps were included. Similarly, all voxels common to wGBC and uGBC in their respective top 10% maps were included in the conjoined 'top 10%' map.

All CCN and DMN regions were included in the conjoined results, with the exception of AIC and aTL. These two regions were present in both the wGBC and uGBC maps, but the regions' voxels did not overlap between the wGBC and uGBC maps. Other regions in the conjunction map include MTG/MOG, VLPFC, right cerebellum, and left M1. The inclusion of left M1, which was not highlighted in the wGBC and uGBC maps due to its small size, is consistent with the location of the M1 'hand' representation and may reflect high connectivity for right hand motor control for the fourteen right-handed subjects.

*wGBC and uGBC distributions*

Graph theoretical investigations into complex systems typically look at unweighted degree distributions, rather than weighted degree distributions. Nonetheless, we were interested in the weighted distribution, since it might reveal something about the organization of connectivity in the brain. Fig. 6A illustrates the group wGBC distribution (top), the comparison to the normal distribution (middle), and the wGBC distribution for two example subjects (bottom). These graphs indicate that the weighted global connectivity of the brain is approximately normally distributed.

The uGBC results lend themselves to more typical graph theory analysis of the degree (number of connections) distribution. Graph theoretic results for complex systems (which have both local clusters and long-range connectivity patterns) typically find degree distributions that are skewed toward high values, while scale-free graphs tend to follow a power law (Amaral et al., 2000; Bullmore and Sporns, 2009). Fig. 6B illustrates the group uGBC distribution (top), the comparison to the normal distribution (middle), and the uGBC distribution for two example subjects (bottom). These results suggest that the brain's global connectivity follows a power law and is skewed toward high values, in turn suggesting that the brain's connectivity is both scale-free and complex. Note, however, that the uGBC threshold of 0.25 (used by Buckner et al., 2009 and also here) is somewhat arbitrary, and that the degree distribution becomes near-normal as this threshold approaches 0 (Fig. 7). Further research is necessary to determine if this reflects the actual degree distribution of the brain or instead an increase in the number of false connections due to noise (which would be expected to be normally distributed).

*Overall GBC patterns*

We created GBC maps summarizing the level of GBC from the top 10% to the top 90% in order to determine the overall pattern of GBC throughout the brain. Fig. 8 illustrates the wGBC pattern, while Fig. 9 illustrates the uGBC pattern. The two patterns are quite similar, with primary sensory-motor cortices having among the lowest and the CCN and DMN having among the highest GBC in both cases. Notable differences between the maps include stronger local clustering for the uGBC map and more subcortical regions for the wGBC map.

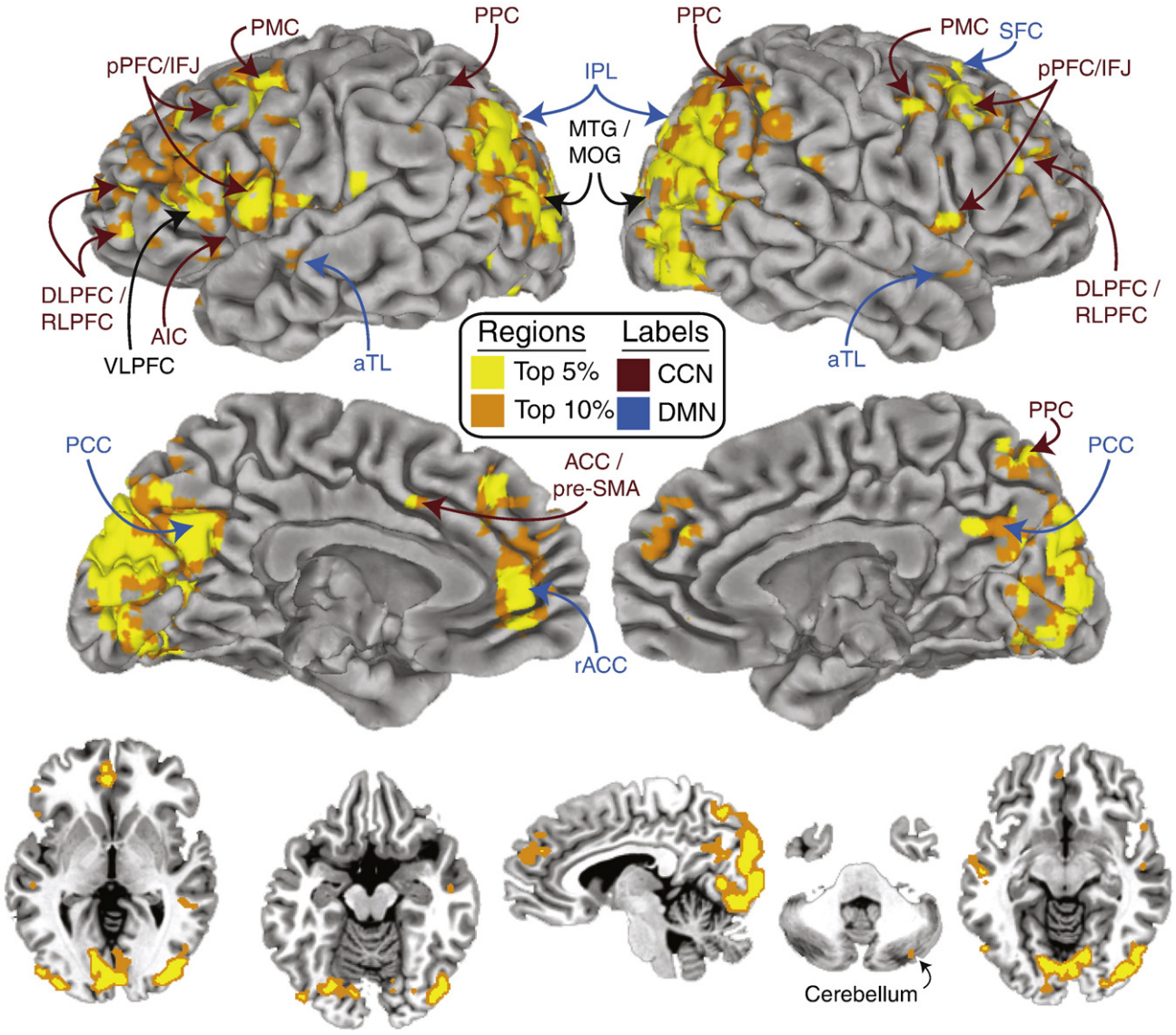


**Fig. 4.** Top percent uGBC regions. The GBC method developed by Buckner et al. (2009) was modified to quantify inter-subject consistency and to indicate the top percentages of voxels. Unlike the wGBC method, the uGBC method uses an unweighted graph, such that the voxel values reflect the concept of *degree* from graph theory. Like the wGBC method, the uGBC method indicates that both the DMN and CCN regions are among the top 5% of voxels. The map was thresholded based on statistical confidence that each voxel is higher than the grand mean across all voxels.

**Table 3**
Top 5% uGBC voxel clusters.

| Cluster labels | Hemisphere | Voxels (3.2 mm$^3$) | % Gray matter | *T*-statistic | Talairach coord: *x* | Talairach coord: *y* | Talairach coord: *z* | Brodmann areas |
|---|---|---|---|---|---|---|---|---|
| PCC, IPL, PPC, precuneus, MTG/MOG | Both | 1393 | 3.29 | 4.3092 | 6.1 | −75.2 | 18.4 | 23,31,39,7,18 |
| PMC | Left | 109 | 0.26 | 4.4035 | −41.2 | 0.1 | 39.4 | 6 |
| DLPFC | Right | 56 | 0.13 | 4.0605 | 39.4 | 26.7 | 22.6 | 46, 9 |
| VLPFC, Broca's area | Left | 48 | 0.11 | 3.9498 | −52.5 | 12.2 | 14.5 | 44, 45 |
| rACC | Left | 36 | 0.09 | 4.0081 | −3.6 | 43.3 | 5.2 | 32 |
| IFJ | Right | 25 | 0.06 | 3.9852 | 44.9 | −0.6 | 24.6 | 6, 9 |
| pPFC | Right | 25 | 0.06 | 4.0788 | 42.2 | 15.4 | 39.7 | 9 |
| PMC | Right | 24 | 0.06 | 3.9138 | 47.1 | −2.1 | 38.1 | 6 |
| RLPFC | Left | 13 | 0.03 | 4.3039 | −38.7 | 45.4 | 6.9 | 10 |
| SFC | Right | 12 | 0.03 | 3.7321 | 18.2 | 37.2 | 41.2 | 8 |
| Medial frontal cortex | Left | 8 | 0.02 | 3.5197 | −2.8 | 34.6 | 40 | 8 |
| AIC | Right | 7 | 0.02 | 3.7189 | 36.8 | 18.6 | 9.9 | 13 |
| IPL | Right | 7 | 0.02 | 3.8329 | 51.4 | −46.3 | 39.1 | 40 |
| PPC, precuneus | Right | 7 | 0.02 | 3.678 | 5.3 | −66.9 | 49.3 | 7 |

Cluster minimum for inclusion in table = 7 voxels. Note that some DMN and CCN regions had fewer than seven voxels remaining, and so are not included here. The percentage of gray matter included in the table equals 4.18%, due to the cluster minimum threshold (i.e., the remaining 0.82% are in clusters with fewer than seven voxels).

**Table 4**
Top 10% uGBC voxel clusters.

| Cluster labels | Hemisphere | Voxels (3.2 mm$^3$) | % Gray matter | *T*-statistic | Talairach coord: *x* | Talairach coord: *y* | Talairach coord: *z* | Brodmann areas |
|---|---|---|---|---|---|---|---|---|
| PCC, IPL, PPC, precuneus, MTG/MOG | Both | 2514 | 5.94 | 3.7715 | 6.1 | −73.6 | 20 | 23,31,39,7,18 |
| RLPFC, DLPFC, PMC, AIC, rACC, SFC | Both (>right) | 663 | 1.57 | 3.3694 | 25.6 | 26.5 | 25.8 | 10, 9, 46, 6, 13, 32, 8 |
| PMC, DLPFC, IFJ, VLPFC | Left | 387 | 0.91 | 3.6355 | −44.6 | 8 | 30.4 | 6, 46, 9, 44, 45 |
| RLPFC | Left | 36 | 0.09 | 3.6065 | −38.6 | 44.6 | 8.2 | 10 |
| VLPFC | Right | 18 | 0.04 | 3.1405 | 53.7 | 7.7 | 5.2 | 44 |
| Superior temporal gyrus | Right | 14 | 0.03 | 3.1937 | 48.1 | −37.9 | 3.1 | 22 |
| aTL | Left | 13 | 0.03 | 3.2802 | −55 | −12.8 | −5.1 | 21, 22 |
| Superior temporal gyrus | Right | 11 | 0.03 | 3.245 | 52.1 | −12 | 11.3 | 22 |
| Superior temporal gyrus | Left | 10 | 0.02 | 3.1232 | −48 | −17.3 | 10.3 | 41 |
| Postcentral gyrus | Left | 9 | 0.02 | 3.3967 | −49.6 | −23.5 | 19.2 | 40 |
| Cerebellum (Crus 2) | Left | 8 | 0.02 | 3.1085 | −30.5 | −69.4 | −41.9 | – |
| IPL | Right | 8 | 0.02 | 3.3561 | 61 | −32.6 | 22.3 | 40 |
| aTL | Right | 7 | 0.02 | 3.3695 | 50 | −12.2 | −8.4 | 22, 21 |
| RLPFC | Left | 7 | 0.02 | 3.3042 | −26.4 | 56.6 | 14.2 | 10 |

Cluster minimum for inclusion in table = 7 voxels. The percentage of gray matter included in the table equals 8.76%, due to the cluster minimum threshold (i.e., the remaining 1.24% are in clusters with fewer than seven voxels).

The uGBC map (Fig. 4) also showed fewer subcortical regions than the wGBC map (Fig. 3) in the top 10%. In order to test the possibility that this was due to processing differences between the two approaches, we systematically reduced these differences to see if more subcortical regions would be present. The differences present in the wGBC map were: (1) the inclusion of low values, (2) the inclusion of negative values, (3) smoothing only after wGBC calculation, and (4) no global mean regression. Accordingly, we created a map using an absolute value of $r>0.15$ threshold (including low positive and negative values), smoothing only after uGBC calculation (6 mm FWHM), and no global mean regression.

These four changes produced minimal differences from the main uGBC map (see Fig. 10). However, uGBC was higher in several subcortical regions (though not nearly as many as in the wGBC map). Specifically, amygdala (mostly on the left), dorsal thalamus (mostly on the left), and cerebellum (same region as in Fig. 4, bilaterally) had higher values due to the changes. When these changes were applied separately, both the difference in threshold and the different use of spatial smoothing affected the uGBC values in subcortical regions (especially in left amygdala).

## Discussion

The wGBC and uGBC methods developed here converge to show that brain regions in the CCN and DMN are among the most globally connected (Figs. 3, 4, and 5). Several other subcortical regions, including amygdala, HC, BG, an MNT region, and cerebellum also have high wGBC (Fig. 3), as expected based on known anatomical connectivity. These findings promise to provide novel insights into the mechanisms of information integration and coordination in the brain.

The first implementation of wGBC analysis was in the context of a previous study of the CCN (Cole and Schneider, 2007). In that study, we pointed out that the CCN is involved in a very large variety of cognitive control tasks and that, given the kinds of complex coordination necessary to implement cognitive control in these many contexts, the CCN is likely to have high global brain connectivity. We showed that the CCN regions are among the most highly globally connected in the brain, which we replicate here (see Fig. 3). However, the previous wGBC analysis method was relatively crude, since it tested only the CCN regions, was based on many short (60 s) rest periods (as opposed to the continuous 10 min rest periods used here), and used large (10 mm$^3$) voxels. The wGBC approach developed here rectifies these issues.

In addition to the CCN, we hypothesized that the DMN would also have among the highest GBC. The logic here is similar: the DMN is involved in a wide variety of domain-general cognitive processes, which likely require connectivity with a large number of other brain regions. Importantly, the tasks that engage the DMN are typically different from those that engage the CCN. For instance, the DMN is more active at rest than during cognitive control tasks (Raichle et al., 2001), is modulated by long-term memory tasks (Buckner et al., 2005), is parametrically modulated by mind wandering (Mason et al., 2007), and is associated with self-reflection (D'Argembeau et al., 2008). We confirmed this hypothesis here, as the DMN (as well as the CCN) regions are among the most globally connected regions (top 5%) both relative to the average uGBC (i.e., the mean degree of connectivity; Fig. 4) and also relative to a wGBC of zero (i.e., no connectivity with other voxels on average; Fig. 3).

We found that the overall pattern of GBC throughout the brain was largely consistent across wGBC (see Fig. 8) and uGBC (see Fig. 9) approaches, and also across several analysis parameters (see Fig. 10). For instance, primary sensory-motor cortices (auditory, visual, somatosensory, motor) consistently had among the lowest GBC values. Further, in accordance with the 'top 10%' maps, even the CCN and DMN voxels below the 'top 10%' threshold nonetheless had among the highest GBC.

In addition to these similarities, there are also notable differences between the maps. For instance, the wGBC map appears to be less spatially clustered (in terms of top percentage GBC) than the uGBC maps. This may reflect the inclusion of more noise by the wGBC method (since low correlations were not removed). Another difference is high wGBC relative to uGBC along the medial wall, which may reflect a small number of very high correlation values (adding little to uGBC but much to wGBC) in these voxels. In contrast, there is high uGBC relative to wGBC along the left lateral frontal cortex, likely reflecting a mixture of positive and negative correlations (i.e., excitatory and inhibitory connections) that 'cancel out' when averaged during the wGBC calculations. Further research is necessary to fully verify these possibilities.

The differential sensitivities of the wGBC and uGBC methods outlined above may also explain why only 14% of the top 10% wGBC and uGBC voxels overlapped (see Fig. 5). For instance, some of the top 10% wGBC voxels may have a small number of very high correlations, making them unlikely to have the large number of connections necessary for the uGBC top 10%. In contrast, some of the top 10% uGBC voxels may have a high number of both positive and negative correlations, making them unlikely to have the consistently positive average connectivity necessary for the wGBC top 10%. Regardless of the reason why many of the 'top ten percent' voxels do not overlap, it is nonetheless informative that there is overlap at all, and that it is largely circumscribed to the hypothesized CCN and DMN regions.

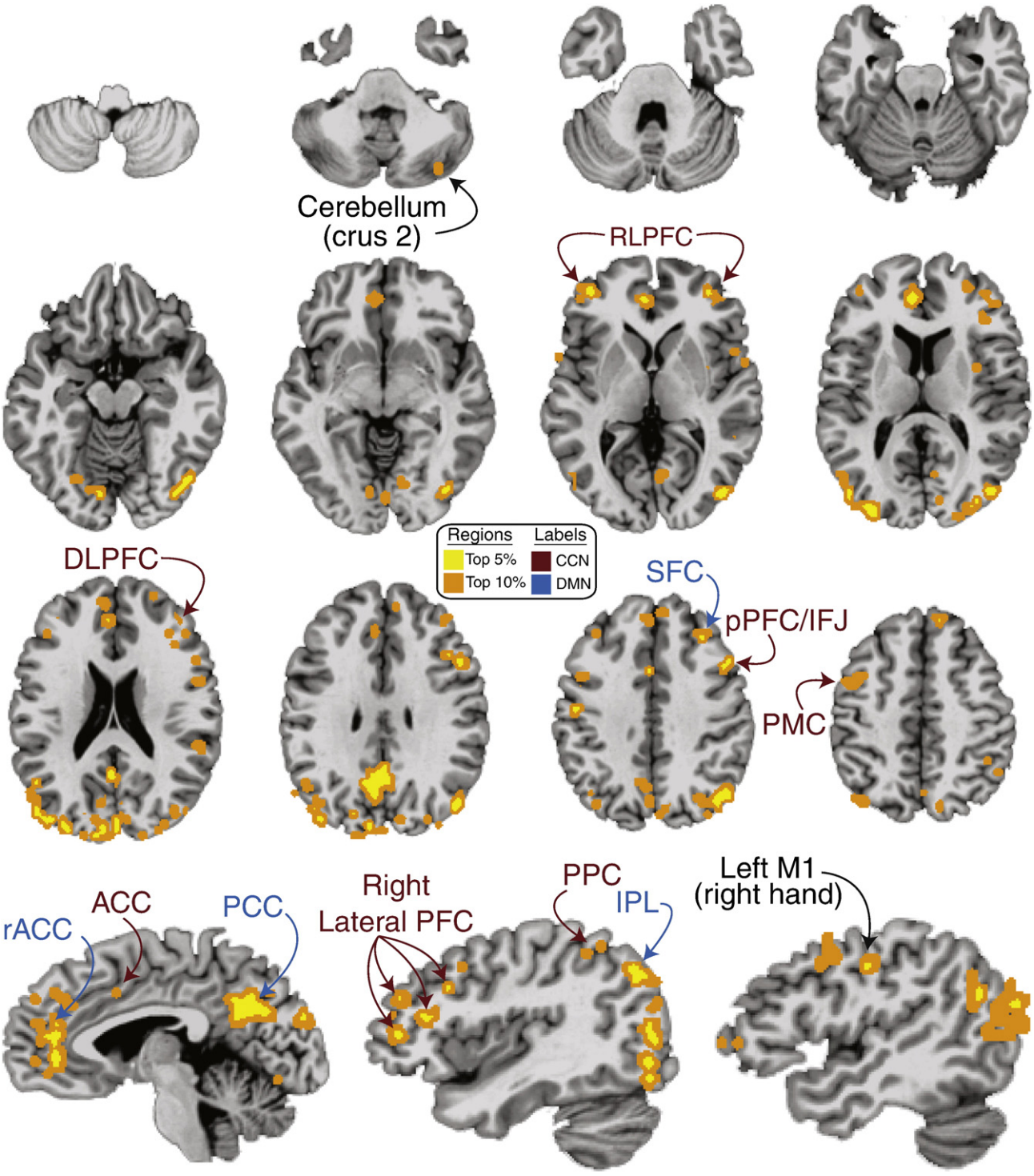


**Fig. 5.** Conjunction of top percent wGBC and uGBC. These regions have both high average connectivity strength (wGBC) *and* high connectivity count (uGBC). Voxels in both the wGBC and uGBC top percent maps are presented in an axial mosaic (12 slices, skipping every eight 1 mm slices), and three sagittal slices. Voxels in both 'top 5%' maps are included in the top 5% here, while voxels in both 'top 10%' maps are included in the top 10%. For instance, the depicted cerebellum region is in the top 5% wGBC, but only the top 10% uGBC, making it in the 'top 10%' here. In actuality, the overlap between the 'top 5%' maps constitutes 1.4% of gray matter. Thus, while most voxels do not overlap between wGBC and uGBC maps, they nonetheless overlap in most of the regions included in the maps. The CCN and DMN regions are labeled, with several additional regions labeled for the purpose of discussion.

The inclusion of subcortical regions known to have extensive connectivity (such as amygdala and thalamus) suggests wGBC may be a more accurate method than uGBC for investigating global connectivity. However, it remains unclear why subcortical regions are present for wGBC and not uGBC. Buckner et al. (2009) noted that more subcortical voxels (in thalamus) were present in their unweighted maps as the connection strength threshold was lowered, perhaps reflecting the possibility that subcortical regions have many weak connections (relative to the strength of connections in cortex) that are removed by the conservative connection strength threshold of 0.25. In contrast, the wGBC method did not remove such weak connections, suggesting the many weak connections in subcortical regions resulted in weighted connectivity values that were quite high on average. Other possibilities for wGBC's success with subcortical regions include

**Table 5**
Conjunction of top percent wGBC and uGBC voxel clusters.

| Cluster labels | Hemisphere | Volume (3.2 mm$^3$) | % Gray matter | Talairach coord: *x* | Talairach coord: *y* | Talairach coord: *z* | Brodmann areas |
|---|---|---|---|---|---|---|---|
| PCC | Both | 100 | 0.24 | −3.3 | −58.6 | 27.5 | 31, 7 |
| MOG/cuneus | Both | 57 | 0.13 | −3 | −84.8 | 23.1 | 18, 19 |
| IPL | Right | 52 | 0.12 | 42.1 | −69.1 | 32.4 | 39 |
| IPL | Left | 49 | 0.12 | −41.7 | −76.4 | 22 | 39 |
| rACC | Both | 44 | 0.10 | −4.7 | 41.6 | 10.3 | 32 |
| MOG | Left | 34 | 0.08 | −30.5 | −85.8 | 14.4 | 18, 19 |
| MOG | Right | 21 | 0.05 | 42.4 | −75.3 | 8.4 | 18, 19 |
| MOG | Right | 20 | 0.05 | 40.1 | −72.7 | −9.1 | 18, 19 |
| pPFC/IFJ | Right | 18 | 0.04 | 46.6 | 13.9 | 29.6 | 9, 6 |
| PMC | Left | 17 | 0.04 | −41.1 | 3.2 | 41.4 | 6 |
| MOG | Right | 16 | 0.04 | 30.7 | −84.1 | 16.6 | 18, 19 |
| DLPFC | Right | 15 | 0.04 | 39.6 | 29.5 | 16.2 | 46, 9 |
| RLPFC | Left | 13 | 0.03 | −37 | 45.6 | 5.6 | 10 |
| PPC/precuneus | Left | 11 | 0.03 | −35 | −70.1 | 41.3 | 7, 19 |
| Lingual gyrus | Left | 10 | 0.02 | −8.7 | −75.3 | −9.7 | 18 |
| MTG | Left | 10 | 0.02 | −46.4 | −60 | 24.4 | 39 |
| RLPFC/DLPFC | Right | 8 | 0.02 | 39.3 | 41.7 | 7.9 | 10, 46 |
| MTG | Left | 7 | 0.02 | −47.3 | −67.3 | 7.7 | 37 |
| RLPFC/DLPFC | Right | 7 | 0.02 | 38.2 | 40.5 | 24.2 | 10, 9 |
| SFC | Right | 6 | 0.01 | 29.9 | 30.5 | 35.6 | 8, 9 |
| SFC | Right | 6 | 0.01 | 11.2 | 39.9 | 43.1 | 8 |

Cluster minimum for inclusion in table = 6 voxels. The voxels overlapping at the top 10% of wGBC and uGBC maps are included. The percentage of gray matter included in the table equals 1.23% while the actual overlap between the 'top 10%' maps was 1.4% of gray matter (this difference was due to the cluster minimum threshold). Note that while most 'top percentage' voxels do not overlap between the wGBC and uGBC maps, the regions included in the overlap are largely consistent with the set of regions in both the source maps.

the lack of spatial smoothing during pre-processing (which may have contaminated subcortical regions with the fMRI signal drop-out in nearby air pockets for uGBC), the inclusion of negative (in addition to positive) correlations, and the lack of global mean regression (which may remove global signals of interest, possibly including signals common to subcortical regions). We verified that these factors affected the presence of subcortical regions in the GBC maps (see Fig. 10), though their effect was small and due mostly to the spatial smoothing and correlation threshold differences. This nonetheless demonstrates that subcortical regions are likely present in the wGBC maps due to their low connectivity (likely modulatory) strengths.

RLPFC was not emphasized in previous GBC studies but was found here to have among the highest GBC. Human postmortem anatomical studies have shown that RLPFC has among the largest dendrites (and associated spines) of any tested brain region (Jacobs et al., 1997; Jacobs et al., 2001), suggesting that RLPFC has many incoming anatomical connections. Such highly convergent connectivity suggests RLPFC may be important for integrating information from across the brain during complex cognitive tasks (Badre, 2008; Botvinick, 2008; Fuster, 2004; Wendelken et al., 2008). This is consistent with the finding that this region has both very high uGBC and very high wGBC (Fig. 5).

The top 5% GBC analyses also revealed several other lateral PFC regions, including DLPFC and pPFC/IFJ (see bottom of Fig. 5). These regions are known to have reciprocal connections with a wide variety of other regions (Bunge et al., 2005; Chafee and Goldman-Rakic, 2000; Fuster et al., 1985), and may serve as intermediates to the more anterior RLPFC (Ramnani and Owen, 2004). Importantly, evidence from non-human primates suggests that these regions are highly interconnected via medial dorsal nucleus in the thalamus (Giguere and Goldman-Rakic, 1988), which was also present in the top 5% wGBC map (see Fig. 3). These results indicate that a network of regions along lateral prefrontal cortex and including the portion of thalamus most interconnected with these regions (medial dorsal nucleus) is highly interconnected with regions throughout the brain, possibly supporting the ability of these regions to maintain and manipulate information from across the brain during complex cognitive control tasks.

The dACC/pSMA is a CCN region with controversy surrounding not only its function but also its exact anatomical location. A recent review illustrated the immense anatomical variability of this region, along with the possibility that the region is area 32′, an anatomically distinct area unique to humans (Cole et al., 2009). The dACC/pSMA region identified here is located on the left cingulate gyrus (see Figs. 5 and 10), which is consistent with area 32′ since this area is typically located on the cingulate gyrus when two cingulate gyri are present, which occurs on the left hemisphere in most individuals (Paus et al., 1996; Vogt et al., 1995). Observing high GBC in what is likely area 32′ is important in that it provides more information regarding possible functions of this evolutionarily recent brain area. Specifically, it appears that this region may be involved in coordinating information across a wide variety of brain areas (given its high GBC) during cognitive control tasks (given its involvement in cognitive control processes (Cole and Schneider, 2007)).

Several researchers have characterized the aTL as a semantic hub able to integrate information from multiple modalities to represent complex objects (Rogers et al., 2006; Rogers et al., 2004; Rogers and Patterson, 2007). Supporting this view, aTL was present in the wGBC map at the top 5% (Fig. 3) and the uGBC map at the top 10% (Fig. 4). However, this region was not present in the wGBC/uGBC conjunction map (Fig. 5). This may reflect lower GBC for this region than other CCN/DMN regions, or it may reflect lower signal (which results in lower correlations) in the region due to fMRI signal drop-out (see Rogers et al., 2006). Future use of methods that can better image aTL with minimal signal drop-out (such as positron emission tomography

**Fig. 6.** Distribution of GBC values. (A) The distribution of the average connectivity strength for all gray matter voxels across 14 individuals (top). The quantile–quantile (Q–Q) plot illustrates that the wGBC values are nearly normally distributed (a perfectly normal distribution would fit the line) (middle). The distributions of all individuals separately were nearly identical to this group distribution, as the two example subjects illustrate (bottom). Note that the values were *z*-normalized in order to aggregate data from all subjects. The grand mean wGBC value across subjects was slightly positive (0.035). (B) The distribution of the degree of connectivity (number of connections with strength greater than 0.25) for all gray matter voxels across 14 individuals (top). The Q–Q plot illustrates that the uGBC values are clearly not normally distributed (middle). The distributions of all individuals separately were nearly identical to this group distribution, as the two example subjects illustrate (bottom).

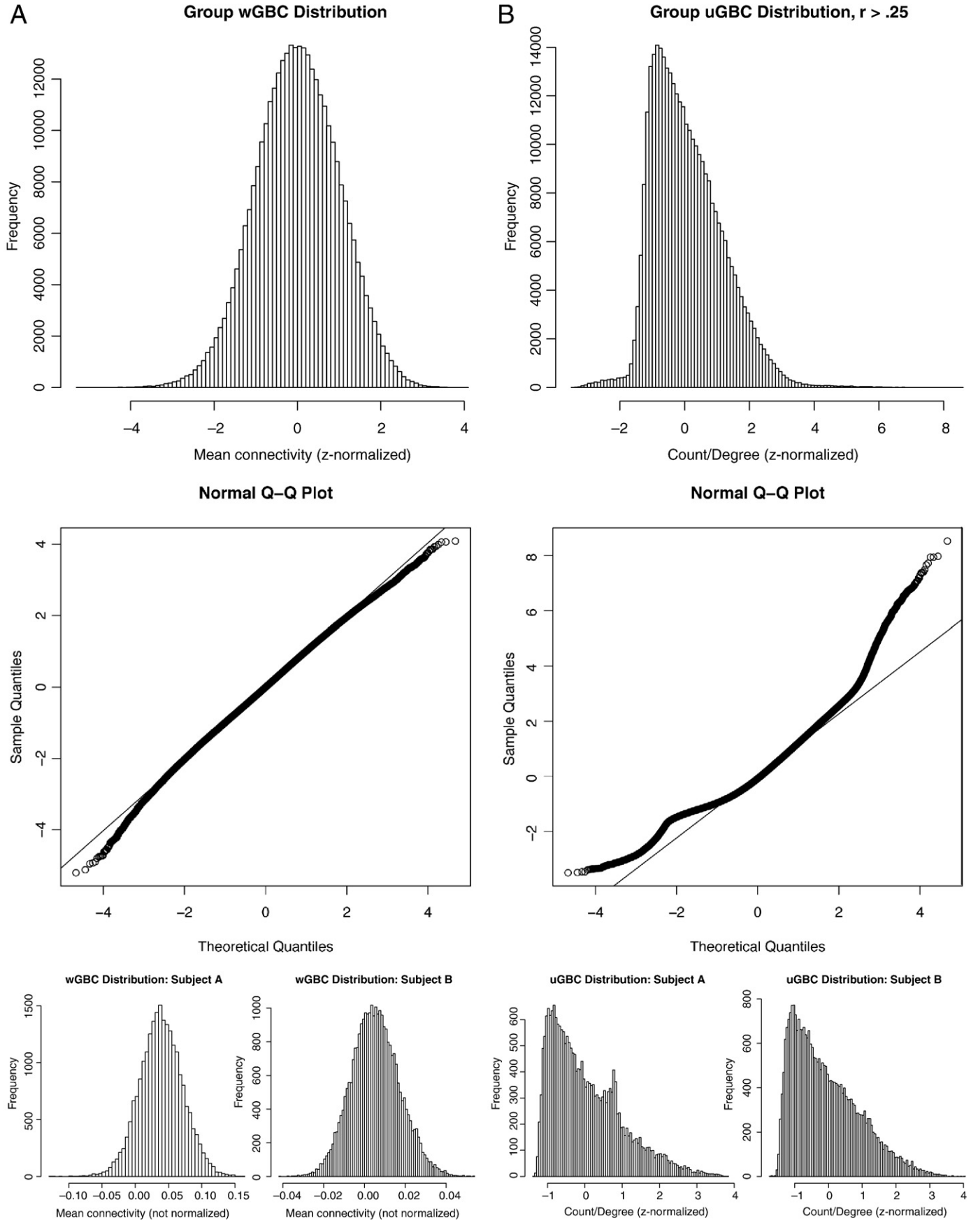
A
Group wGBC Distribution
Frequency
Mean connectivity (z-normalized)
B
Group uGBC Distribution, r > .25
Frequency
Count/Degree (z-normalized)
Normal Q–Q Plot
Sample Quantiles
Theoretical Quantiles
Normal Q–Q Plot
Sample Quantiles
Theoretical Quantiles
wGBC Distribution: Subject A
Frequency
Mean connectivity (not normalized)
wGBC Distribution: Subject B
Frequency
Mean connectivity (not normalized)
uGBC Distribution: Subject A
Frequency
Count/Degree (z-normalized)
uGBC Distribution: Subject B
Frequency
Count/Degree (z-normalized)

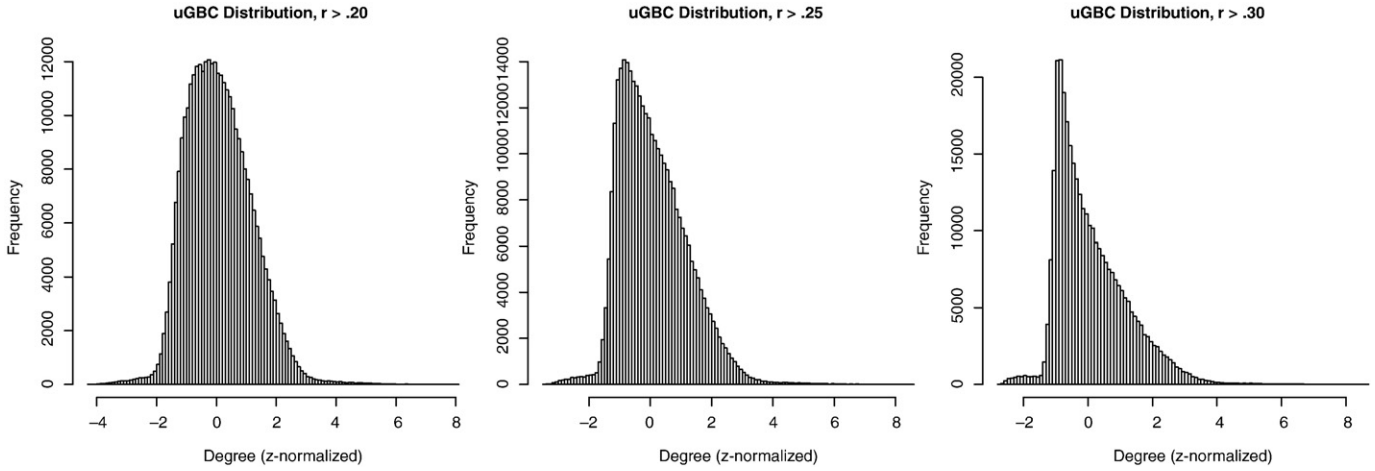


**Fig. 7.** uGBC distributions across different connection strength thresholds. Since the 0.25 connection strength threshold (used by Buckner et al., 2009 and also here) is somewhat arbitrary, we investigated distributions across several thresholds. As the connection strength threshold is increased, the uGBC distribution is seen to better obey a power law. In contrast, as the connection strength threshold is decreased, the uGBC distribution is seen to become more symmetrical, resembling a normal distribution. This pattern may be due to either greater accuracy at lower thresholds (i.e., the high thresholds are removing important low-strength connections) or greater accuracy at higher thresholds (i.e., the low thresholds retain connections that are not real and have non-zero correlation values due to noise). Further research is necessary to distinguish between these two possibilities.

(PET)) may help resolve this issue. It is also possible that different portions of aTL are differentially sensitive to wGBC versus uGBC (see Figs. 3 and 4).

For the most part, primary sensory and motor cortices had low GBC. A clear exception, however, was left M1 (see Fig. 5). This region's location is consistent with the motor representation of the right hand, suggesting that the region may have high GBC due to the right-handedness of all 14 subjects. Future research, possibly involving GBC analysis of both right- and left-handed individuals, is necessary to fully verify if handedness is the product of differentially high GBC (i.e., high global connectivity for the dominant hand relative to the non-dominant hand).

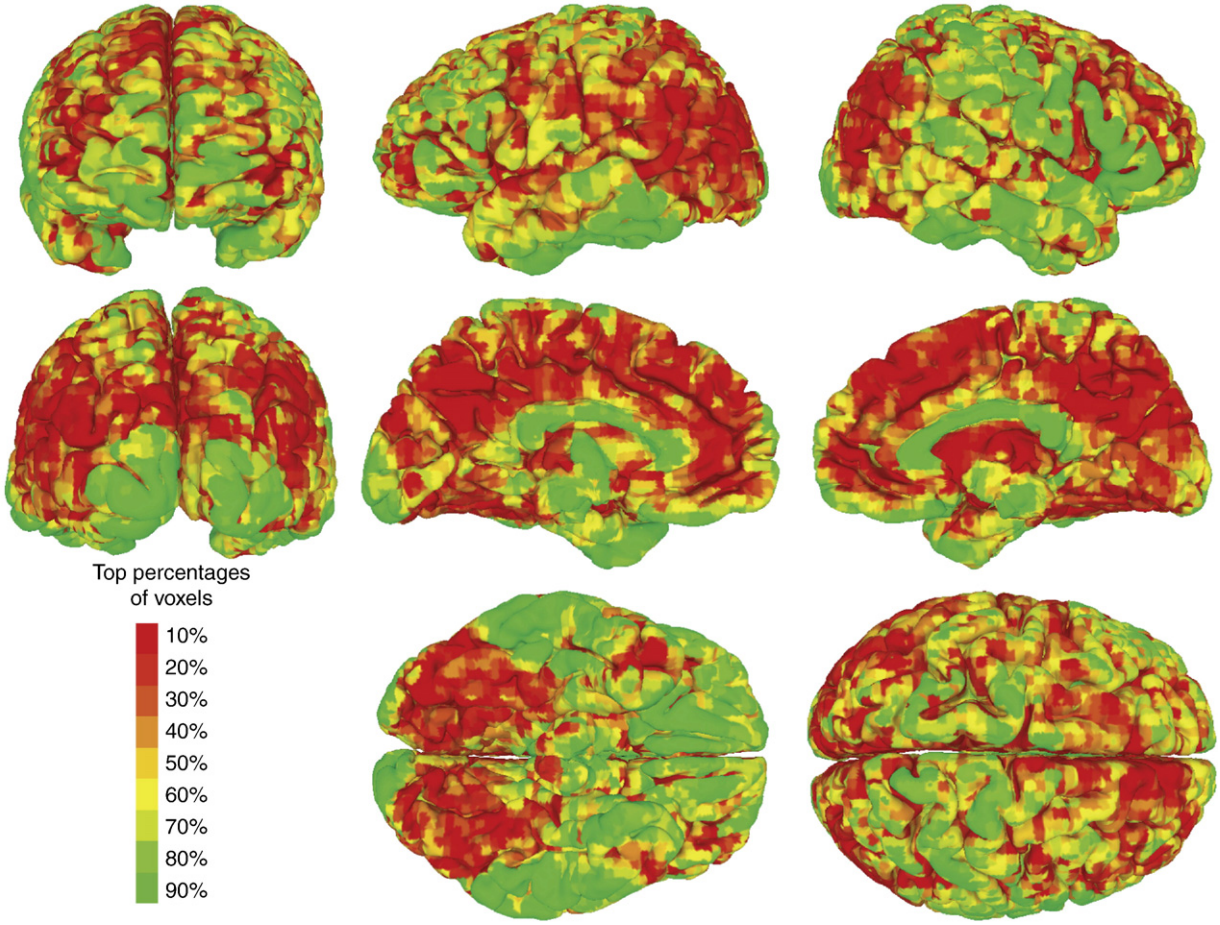


**Fig. 8.** Overall wGBC by top percentages of voxels. Voxels were colored according to their inclusion in the top percentages of voxels. The map is based on group *F*-statistics and so reflects the wGBC strength and consistency of each voxel relative to 0 wGBC. Note that the 'top 90%' also includes the remaining 10% in order to include all voxels.

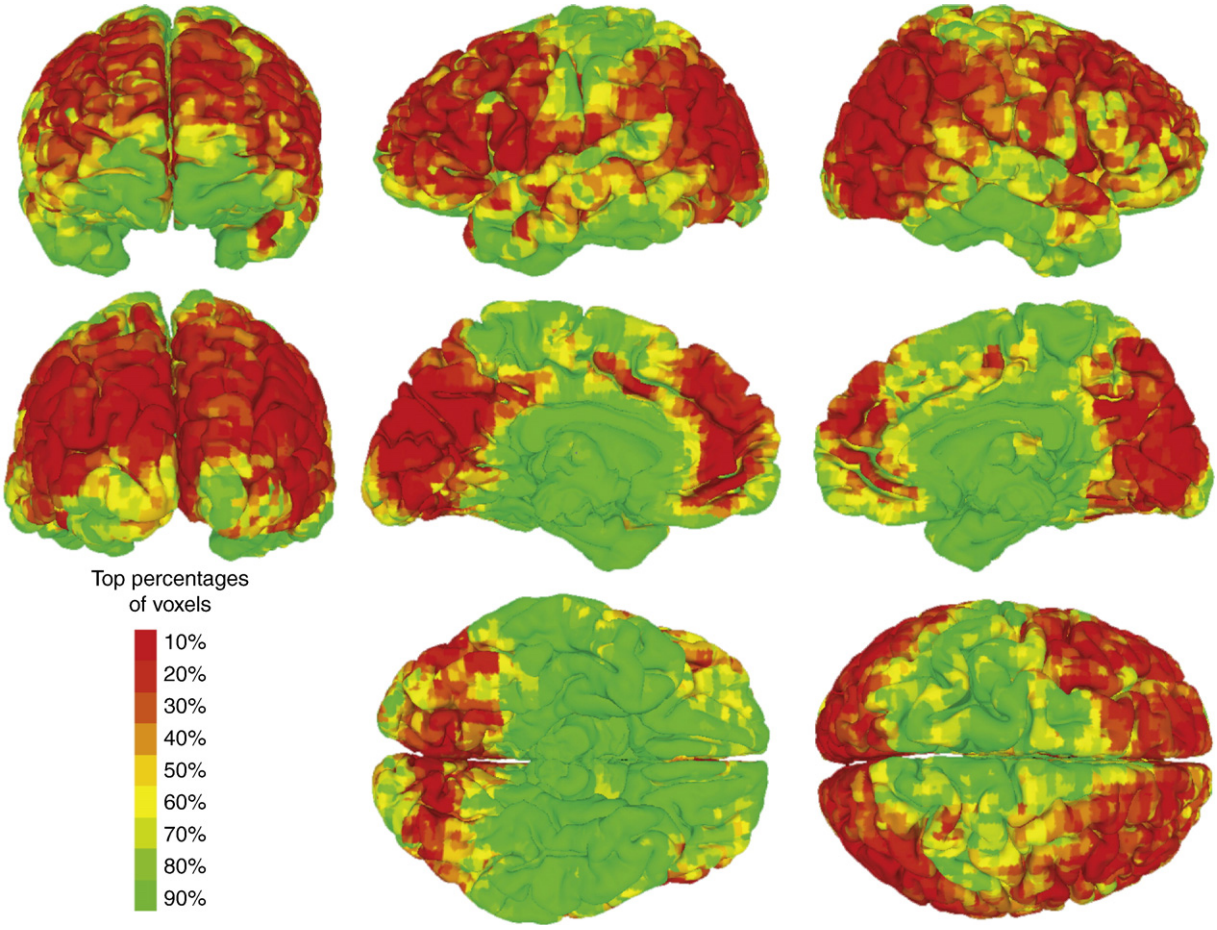


**Fig. 9.** Overall uGBC by top percentages of voxels. Like Fig. 8, voxels were colored according to their inclusion in the top percentages of voxels. The map is based on group *F*-statistics and so reflects the uGBC count and consistency of each voxel relative to the mean uGBC value. The values above the 50% threshold reflect statistical significance above the mean, while values below the 50% threshold reflect statistical significance below the mean.

A recent study using rs-fcMRI reported that portions of cerebellum connect to distinct portions of frontal cortex in humans (Krienen and Buckner, 2009). Specifically, they found that portions of cerebellum that were connected to motor cortex were distinct from portions connected to prefrontal cortex. The wGBC map includes a large part of cerebellum as among the most highly connected regions in the brain (top 5%). The uGBC map includes two small regions in cerebellum (top 10%). These wGBC and uGBC cerebellar regions are largely consistent with the portions of cerebellum Krienen and Buckner (2009) found to be connected to DLPFC, medial prefrontal cortex, and (to a lesser extent) RLPFC. Notably, very little of the portion connecting to motor cortex was present in the GBC maps. These findings support the conclusion that portions of cerebellum with high GBC have that GBC due to connectivity with cortical regions with high GBC, such as the prefrontal regions within the CCN and DMN.

In addition to subcortical, CCN, and DMN regions, several visual regions were also among the most globally connected. This may reflect the privileged placement of visual processing in the human brain (Ungerleider and Haxby, 1994). Future research is necessary to determine if this high GBC is due to the relatively large size of visual cortex (thus comprising a disproportionately large number of voxels) or if it is due to high connectivity with regions outside visual cortex as well.

Graph theory has been utilized to great effect in recent studies of brain connectivity. Overlapping with the graph theory concepts of hubs and node centrality, the present study uses uGBC and wGBC to determine the most highly connected brain regions. A recent study used graph theory in the context of diffusion weighted MRI (DWI) to investigate global anatomical connectivity (Hagmann et al., 2008). That study's findings largely agree with the present study's findings, showing that RLPFC, PCC, rACC, and IPL have high global connectivity. However, that study showed that PCC (including a portion of the precuneus) had the highest global connectivity of any region. We also found especially high connectivity in this region, suggesting that the functional connectivity approach used here reflects underlying anatomical connectivity to some extent. Note, however, that functional connectivity may be more relevant to understanding how regional connections influence brain dynamics and ultimately behavior, since it can include strong indirect connections (which are likely highly relevant to brain dynamics) as well as direct connections.

The lack of an arbitrary threshold during wGBC map creation is a potential advantage of wGBC relative to uGBC. Indeed, while Buckner et al. (2009) demonstrated similar spatial maps at a variety of strength thresholds for uGBC, we also found that the uGBC distribution changes dramatically with different strength thresholds (Fig. 7). This throws some doubt on the appropriateness of any particular uGBC strength threshold. Further research is necessary to determine if the tendency toward symmetry at lower strength thresholds reflects the actual degree distribution of the brain or instead an increase in the number of false connections due to noise. One possible solution may be to threshold connections in a principled manner using a recently-developed method for quantifying the statistical certainty of connectivity (Kramer et al., 2009). Note that the uGBC maps are likely informative regarding the regions with the highest GBC even if a given threshold is not appropriate for characterizing the degree distribution of the brain.

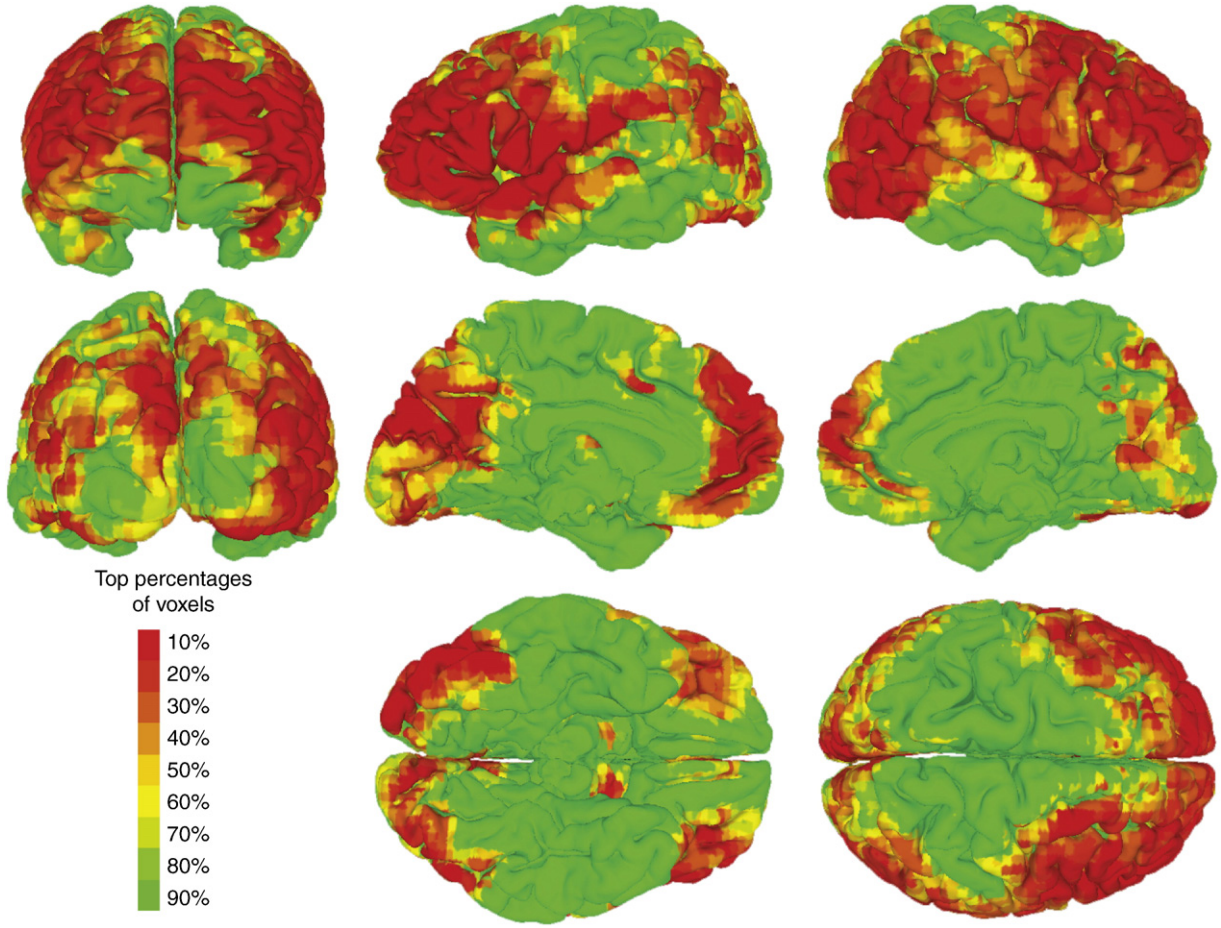


**Fig. 10.** Overall uGBC with fewer processing differences from wGBC. Like Fig. 9, voxels were colored according to their inclusion in the top percentages of voxels. The following changes were made when creating this map in order to better approximate the methods used for the wGBC map: (1) low values were included ($r$>0.15), (2) negative values were included (also, $r$<-0.15), (3) spatial smoothing was applied only after uGBC calculation, and (4) global mean regression was not used.

Since there is no *a priori* reason to assume that the brain's connectivity is normally distributed, it is possible that the actual distribution of uGBC values is a non-normal power law distribution as found at higher thresholds (see Fig. 7). Indeed, previous estimates of the degree distribution of the brain (the graph theory equivalent of the uGBC distribution) have also been power law distributions, implying the human brain is 'scale free' and forms a small world network (Bullmore and Sporns, 2009; Heuvel et al., 2008). However, our results illustrate that this may be a premature conclusion, as the threshold used prior to estimating the degree distribution has a substantial effect on its shape. This same problem extends to estimates using anatomical connectivity as measured by DWI since many smaller fiber connections (e.g., in gray matter) that may constitute the lower end of a normal distribution are lost in noise with current DWI methods (Gigandet et al., 2008). Further research is necessary to reduce noise in these global connectivity approaches in order to see the true degree distribution of the human brain.

Several forms of noise common to fMRI experiments may have affected the results presented here. For instance, fMRI signal drop-out is known to occur near the sinuses and other air pockets, and may have reduced correlations in surrounding gray matter. Indeed, there was a tendency in the results reported here for low GBC in orbitofrontal cortex and inferior temporal lobes, among other regions near air pockets (see Figs. 8 and 9). Further research is necessary to determine the effects of signal drop-out on estimates of GBC. Another potential source of noise was the presence of cardiac and respiratory correlations. We tested the effect of such artifactual correlations using global mean regression, and found that they had little effect on the group results. However, several individual subjects showed high wGBC and uGBC values in parts of the brain that typically correlate with respiratory and cardiac artifacts due to nearby blood vessels (Birn et al., 2006). Further research (possibly involving regression of nuisance cardiac and respiratory signals) is necessary to determine the effect of physiological artifacts on GBC estimates.

It is perhaps surprising that the CCN and DMN were *both* among the top 5% of globally connected voxels given that their activities are not typically correlated with each other (Fox et al., 2005; Murphy et al., 2008). However, they do share one thing in common: their activities are not correlated with the external world either. Evidence for this comes from a study of brain activity during movie watching (Hasson et al., 2004), which found that almost the entire brain correlated between subjects when watching the same movie, except for many of the CCN and DMN regions. This result, in conjunction with the present study's results, suggests that the CCN and DMN are able to utilize their extensive connectivity to integrate information from primary sensory regions and also between their own regions internally to form an internal 'mental' world that may characterize the core of human experience. Future research may reveal the exact connectivity patterns and neural processes that make the emergent properties of this internal 'mental' world (e.g., selfhood, consciousness) possible. Additionally, further research may reveal the similarities and differences between the CCN and DMN connectivity patterns, perhaps revealing the mechanism of their differentiation despite both having high global connectivity.

It is also potentially surprising that the CCN and DMN are within the top 5% of *both* the uGBC and wGBC statistics despite the different distributions underlying these two approaches (see Fig. 5). The wGBC values are normally distributed for both the group and individual subjects (Fig. 6A), while the uGBC values resemble a power law distribution (Fig. 6B). However, both distributions have a high-value tail that gradually decreases. The similarity of the top GBC values using the two approaches indicates that these high-value tails include many of the same voxels, solidifying the conclusion that the regions including these voxels are among the most globally connected portions of the brain.

In summary, we developed two new methods, uGBC and wGBC analysis, which showed that the brain's most globally interactive regions can be placed within the context of known large-scale networks. These networks include the CCN and DMN, whose regions are highly internally correlated during both rest and performance of a wide variety of tasks (Cole and Schneider, 2007; Fox et al., 2005; Toro et al., 2008). Other networks with high wGBC include amygdala, HC, BG loops with cortex, and cerebellar loops with cortex, among others. The high global connectivity found for these networks implies importance in complex cognitive functions that require extensive interactive processing across the brain, which is largely consistent with the putative functions of these networks. A key challenge for further research is to characterize exactly how these particularly important networks' connectivity patterns contribute to cognition and behavior.

## Acknowledgments

We thank Bruna Martins for insightful comments and suggestions. We would also like to thank Robert Cox and Kyle Simmons for developing efficient global connectivity software. This research was supported by DARPA. The findings and opinions contained here are those of the authors, not DARPA. M.C. was supported by an NSF graduate research fellowship.

## References

Achard, S., Salvador, R., Whitcher, B., Suckling, J., Bullmore, E., 2006. A resilient, low-frequency, small-world human brain functional network with highly connected association cortical hubs. J. Neurosci. 26, 63–72.

Amaral, L.A., Scala, A., Barthelemy, M., Stanley, H.E., 2000. Classes of small-world networks. Proc. Natl. Acad. Sci. U.S.A. 97, 11149–11152.

Badre, D., 2008. Cognitive control, hierarchy, and the rostro-caudal organization of the frontal lobes. Trends Cogn. Sci. 12, 193–200.

Barbas, H., 2000. Connections underlying the synthesis of cognition, memory, and emotion in primate prefrontal cortices. Brain Res. Bull. 52, 319–330.

Behrens, T.E., Johansen-Berg, H., Woolrich, M.W., Smith, S., Wheeler-Kingshott, C.A., Boulby, P.A., Barker, G.J., Sillery, E.L., Sheehan, K., Ciccarelli, O., Thompson, A.J., Brady, J.M., Matthews, P.M., 2003. Non-invasive mapping of connections between human thalamus and cortex using diffusion imaging. Nat. Neurosci. 6, 750–757.

Birn, R.M., Diamond, J.B., Smith, M.A., Bandettini, P.A., 2006. Separating respiratory-variation-related fluctuations from neuronal-activity-related fluctuations in fMRI. NeuroImage 31, 1536–1548.

Botvinick, M.M., 2008. Hierarchical models of behavior and prefrontal function. Trends Cogn. Sci. 12, 201–208.

Buckner, R.L., Snyder, A.Z., Shannon, B.J., LaRossa, G., Sachs, R., Fotenos, A.F., Sheline, Y.I., Klunk, W.E., Mathis, C.A., Morris, J.C., Mintun, M.A., 2005. Molecular, structural, and functional characterization of Alzheimer's disease: evidence for a relationship between default activity, amyloid, and memory. J. Neurosci. 25, 7709–7717.

Buckner, R.L., Sepulcre, J., Talukdar, T., Krienen, F.M., Liu, H., Hedden, T., Andrews-Hanna, J.R., Sperling, R.A., Johnson, K.A., 2009. Cortical hubs revealed by intrinsic functional connectivity: mapping, assessment of stability, and relation to Alzheimer's disease. J. Neurosci. 29, 1860–1873.

Bullmore, E., Sporns, O., 2009. Complex brain networks: graph theoretical analysis of structural and functional systems. Nat. Rev. Neurosci. 10, 186–198.

Bunge, S.A., Wallis, J.D., Parker, A., Brass, M., Crone, E.A., Hoshi, E., Sakai, K., 2005. Neural circuitry underlying rule use in humans and nonhuman primates. J. Neurosci. 25, 10347–10350.

Chafee, M.V., Goldman-Rakic, P.S., 2000. Inactivation of parietal and prefrontal cortex reveals interdependence of neural activity during memory-guided saccades. J. Neurophysiol. 83, 1550–1566.

Cole, M.W., Schneider, W., 2007. The cognitive control network: integrated cortical regions with dissociable functions. Neuroimage 37, 343–360.

Cole, M.W., Yeung, N., Freiwald, W.A., Botvinick, M., 2009. Cingulate cortex: diverging data from humans and monkeys. Trends in Neurosciences 32 (11), 566–574.

Cox, R.W., 1996. AFNI: software for analysis and visualization of functional magnetic resonance neuroimages. Comput. Biomed. Res. 29, 162–173.

D'Argembeau, A., Feyers, D., Majerus, S., Collette, F., Van der Linden, M., Maquet, P., Salmon, E., 2008. Self-reflection across time: cortical midline structures differentiate between present and past selves. Soc. Cogn. Affect. Neurosci. 3, 244–252.

Dale, A.M., Fischl, B.R., Sereno, M.I., 1999. Cortical surface-based analysis: I. Segmentation and surface reconstruction. Neuroimage 9, 179–194.

Deuker, L., Bullmore, E.T., Smith, M., Christensen, S., Nathan, P.J., Rockstroh, B., Bassett, D.S., 2009. Reproducibility of graph metrics of human brain functional networks. Neuroimage 47, 1460–1468.

Dosenbach, N.U.F., Visscher, K.M., Palmer, E.D., Miezin, F.M., 2006. A core system for the implementation of task sets. Neuron 50 (5), 799–812.

Eichenbaum, H., Yonelinas, A.P., Ranganath, C., 2007. The medial temporal lobe and recognition memory. Ann. Rev. Neurosci. 30, 123–152.

Fair, D.A., Schlaggar, B.L., Cohen, A.L., Miezin, F.M., Dosenbach, N.U.F., Wenger, K.K., Fox, M. D., Snyder, A., Raichle, M.E., Petersen, S.E., 2007. A method for using blocked and event-related fMRI data to study "resting state" functional connectivity. Neuroimage 35, 396–405.

Fischl, B., Salat, D.H., Busa, E., Albert, M., Dieterich, M., Haselgrove, C., van der Kouwe, A., Killiany, R., Kennedy, D., Klaveness, S., Montillo, A., Makris, N., Rosen, B., Dale, A.M., 2002. Whole brain segmentation: automated labeling of neuroanatomical structures in the human brain. Neuron 33, 341–355.

Fischl, B., Salat, D.H., van der Kouwe, A.J., Makris, N., Ségonne, F., Quinn, B.T., Dale, A.M., 2004. Sequence-independent segmentation of magnetic resonance images. Neuroimage 23 (Suppl. 1), S69–S84.

Fox, M.D., Snyder, A.Z., Vincent, J.L., Corbetta, M., Van Essen, D.C., Raichle, M.E., 2005. The human brain is intrinsically organized into dynamic, anticorrelated functional networks. Proc. Natl. Acad. Sci. U.S.A. 102, 9673–9678.

Fox, M., Zhang, D., Snyder, A., Raichle, M., 2009. The global signal and observed anticorrelated resting state brain networks. J. Neurophysiol. 101, 3270–3283.

Fuster, J.M., 2004. Upper processing stages of the perception–action cycle. Trends. Cogn. Sci. 8, 143–145.

Fuster, J.M., Bauer, R.H., Jervey, J.P., 1985. Functional interactions between inferotemporal and prefrontal cortex in a cognitive task. Brain Res. 330, 299–307.

Genovese, C.R., Lazar, N.A., Nichols, T., 2002. Thresholding of statistical maps in functional neuroimaging using the false discovery rate. Neuroimage 15, 870–878.

Gigandet, X., Hagmann, P., Kurant, M., Cammoun, L., Meuli, R., Thiran, J.P., 2008. Estimating the confidence level of white matter connections obtained with MRI tractography. PLoS ONE 3, e4006.

Giguere, M., Goldman-Rakic, P.S., 1988. Mediodorsal nucleus: areal, laminar, and tangential distribution of afferents and efferents in the frontal lobe of rhesus monkeys. J. Comp. Neurol. 277, 195–213.

Golanov, E.V., Yamamoto, S., Reis, D.J., 1994. Spontaneous waves of cerebral blood flow associated with a pattern of electrocortical activity. Am. J. Physiol. Regul. 266 (1 Pt 2), R204–R214.

Goldman, R.I., Stern, J.M., Engel, J., Cohen, M.S., 2002. Simultaneous EEG and fMRI of the alpha rhythm. Neuroreport 13, 2487–2492.

Griswold, M.A., Jakob, P.M., Heidemann, R.M., Nittka, M., Jellus, V., Wang, J., Kiefer, B., Haase, A., 2002. Generalized autocalibrating partially parallel acquisitions (GRAPPA). Magnetic Reson. Med.: Official J. Soc. Magn. Reson. Med./Soc. Magn. Reson. Med. 47, 1202–1210.

Hagmann, P., Cammoun, L., Gigandet, X., Meuli, R., Honey, C., Wedeen, V., Sporns, O., Friston, K.J., 2008. Mapping the structural core of human cerebral cortex. Plos Biol. 6, e159.

Hasson, U., Nir, Y., Levy, I., Fuhrmann, G., Malach, R., 2004. Intersubject synchronization of cortical activity during natural vision. Science 303, 1634–1640.

Herlenius, E., Lagercrantz, H., 2004. Development of neurotransmitter systems during critical periods. Exp. Neurol. 190 (Suppl. 1), S8–S21.

Heuvel, M.v.d., Stam, C., Boersma, M., Pol, H.H., 2008. Small-world and scale-free organization of voxel-based resting-state functional connectivity in the human brain. Neuroimage 43, 528–539.

Jacobs, B., Driscoll, L., Schall, M., 1997. Life-span dendritic and spine changes in areas 10 and 18 of human cortex: a quantitative Golgi study. J. Comp. Neurol. 386, 661–680.

Jacobs, B., Schall, M., Prather, M., Kapler, E., Driscoll, L., Baca, S., Jacobs, J., Ford, K., Wainwright, M., Treml, M., 2001. Regional dendritic and spine variation in human cerebral cortex: a quantitative Golgi study. Cereb. Cortex 11, 558–571.

Jolkkonen, E., Pitkänen, A., 1998. Intrinsic connections of the rat amygdaloid complex: projections originating in the central nucleus. The. J. Comp. Neurol. 395, 53–72.

Kannurpatti, S., Biswal, B.B., Kim, Y., Rosen, B.R., 2008. Spatio-temporal characteristics of low-frequency BOLD signal fluctuations in isoflurane-anesthetized rat brain. Neuroimage 40, 1738–1747.

Kelly, R.M., Strick, P.L., 2003. Cerebellar loops with motor cortex and prefrontal cortex of a nonhuman primate. J. Neurosci. 23, 8432–8444.

Kramer, M., Eden, U., Cash, S., Kolaczyk, E., 2009. Network inference with confidence from multivariate time series. Phys. Rev. E. 79, 1–13.

Krienen, F., Buckner, R., 2009. Segregated fronto-cerebellar circuits revealed by intrinsic functional connectivity. Cereb. Cortex 1–13.

Lancaster, J.L., Woldorff, M.G., Parsons, L.M., Liotti, M., Freitas, C.S., Rainey, L., Kochunov, P.V., Nickerson, D., Mikiten, S.A., Fox, P.T., 2000. Automated Talairach atlas labels for functional brain mapping. Hum. Brain Mapp. 10, 120–131.

Mason, M., Norton, M., Van Horn, J., Wegner, D., Grafton, S., Macrae, C., 2007. Wandering minds: the default network and stimulus-independent thought. Science 315, 393–395.
Middleton, F.A., Strick, P.L., 1994. Anatomical evidence for cerebellar and basal ganglia involvement in higher cognitive function. Science 266, 458–461.
Murphy, K., Birn, R., Handwerker, D.A., Jones, T., Bandettini, P.A., 2008. The impact of global signal regression on resting state correlations: are anti-correlated networks introduced? Neuroimage 44 (3), 893–905.
Paus, T., Tomaiuolo, F., Otaky, N., MacDonald, D., Petrides, M., Atlas, J., Morris, R., Evans, A.C., 1996. Human cingulate and paracingulate sulci: pattern, variability, asymmetry, and probabilistic map. Cereb. Cortex 6, 207–214.
Kandel, E.R., Schwartz, J.H., Jessell, T.M. (Eds.), 2000. Principles of neural science. The McGraw-Hill Companies.
Squire, L.R., McConnell, S.K., Zigmond, M.J. (Eds.), 2003. Fundamental neuroscience. Elsevier.
Raichle, M.E., MacLeod, A.M., Snyder, A.Z., Powers, W.J., Gusnard, D.A., Shulman, G.L., 2001. A default mode of brain function. Proc. Natl. Acad. Sci. U.S.A. 98, 676–682.
Ramnani, N., Owen, A., 2004. Anterior prefrontal cortex: insights into function from anatomy and neuroimaging. Nat. Rev. Neurosci. 5, 184–194.
Rogers, T.T., Patterson, K., 2007. Object categorization: reversals and explanations of the basic-level advantage. J. Exp. Psychol: Gen. 136, 451–469.
Rogers, T.T., Lambon Ralph, M.A., Garrard, P., Bozeat, S., McClelland, J.L., Hodges, J.R., Patterson, K., 2004. Structure and deterioration of semantic memory: a neuropsychological and computational investigation. Psychol. Rev. 111, 205–235.
Rogers, T.T., Hocking, J., Noppeney, U., Mechelli, A., Gorno-Tempini, M.L., Patterson, K., Price, C.J., 2006. Anterior temporal cortex and semantic memory: reconciling findings from neuropsychology and functional imaging. Cogn. Affect. Behav. Neurosci. 6, 201–213.
Salvador, R., Suckling, J., Coleman, M.R., Pickard, J.D., Menon, D., Bullmore, E., 2005a. Neurophysiological architecture of functional magnetic resonance images of human brain. Cereb. Cortex 15, 1332–1342.
Salvador, R., Suckling, J., Schwarzbauer, C., Bullmore, E., 2005b. Undirected graphs of frequency-dependent functional connectivity in whole brain networks. Philos. Trans. R. Soc. Lond. B. Biol. Sci. 360, 937–946.
Sporns, O., Honey, C., Kötter, R., Kaiser, M., 2007. Identification and classification of hubs in brain networks. PLoS ONE 2, e1049.
Talairach, J., Tournoux, P., 1988. Co-planar stereotaxic atlas of the human brain. Thieme.
R Development Core Team, 2008. R: a language and environment for statistical computing Vienna, Austria. ISBN 3-900051-07-0, URL http://www.R-project.org.
Toro, R., Fox, P., Paus, T., 2008. Functional coactivation map of the human brain. Cereb. Cortex 18, 2553–2559.
Ungerleider, L.G., Haxby, J.V., 1994. 'What' and 'where' in the human brain. Curr. Opin. Neurobiol. 4, 157–165.
Van Essen, D.C., 2004. Surface-based approaches to spatial localization and registration in primate cerebral cortex. Neuroimage 23 (Suppl. 1), S97–S107.
Vincent, J.L., Patel, G.H., Fox, M.D., Snyder, A., Baker, J.T., Van Essen, D.C., Zempel, J.M., Snyder, L.H., Corbetta, M., Raichle, M.E., 2007. Intrinsic functional architecture in the anaesthetized monkey brain. Nature 447, 83–86.
Vogt, B.A., Nimchinsky, E.A., Vogt, L.J., Hof, P.R., 1995. Human cingulate cortex: surface features, flat maps, and cytoarchitecture. J. Comp. Neurol. 359, 490–506.
Wendelken, C., Nakhabenko, D., Donohue, S.E., Carter, C.S., Bunge, S.A., 2008. "Brain is to thought as stomach is to ??": investigating the role of rostrolateral prefrontal cortex in relational reasoning. J. Cogn. Neurosci. 20, 682–693.